5-2021

Validation of Arterial Distensibility Neural Network Model with Clinical Data

Cassondra Michelle Petersen

Validation of Arterial Distensibility Neural Network Model with Clinical Data

by

Cassondra Michelle Petersen

A thesis submitted to the College of Engineering and Science of
Florida Institute of Technology
in partial fulfillment of the requirements
for the degree of

Master of Science
in
Biomedical Engineering

Melbourne, Florida
May, 2021

We the undersigned committee hereby approve the attached thesis,

"Validation of Arterial Distensibility Neural Network Model with Clinical Data."

by

Cassondra Michelle Petersen

_____

Mehmet Kaya, Ph.D.
Associate Professor
Biomedical and Chemical Engineering and Sciences
Major Advisor

_____

Diego Guarin Lopez, Ph.D.
Assistant Professor
Biomedical and Chemical Engineering and Sciences
Committee Member

_____

Ersoy Subasi, Ph.D.
Assistant Professor
Computer Engineering and Sciences
Committee Member

_____

Andrew Knight, Ph.D.
Professor and Department Head
Biomedical and Chemical Engineering and Sciences

Abstract

Title: Validation of Arterial Distensibility Neural Network Model with Clinical Data

Author: Cassondra Michelle Petersen

Advisor: Mehmet Kaya, Ph.D.

Cardiovascular diseases continue to plague the world as the number one killer of adults each year. As cardiovascular diseases can start with seemingly no symptoms, heart disease has been coined as the silent killer. With the ongoing COVID-19 global pandemic, the need for advances in cardiovascular advances has become even more prevalent as this virus is known to cause more severe damage to those who have underlying cardiovascular problems. These two reasons show the dire clinical need for researchers to continue to use novel techniques such as neural networks to find new approaches for helping physicians non-invasively and quickly add predictive technologies into their routine practices to evaluate a patient's risk of developing any cardiovascular diseases. The cardiovascular system has historically been hard to replicate using computational flow fluid dynamic software as it is one of the most complex flow systems. Over the years, changes in aortic diameter, blood pressure (BP), and arterial compliance have all been identified as indicators of cardiovascular diseases in humans. Thus, being able to routinely monitor aortic

diameter size can help detect a cardiovascular disease sooner and potentially help physicians find meaningful solutions to prevent the progression of these diseases.

Currently, there is no approved or widely accepted non-invasive neural network (NN) technology for determining the risk of developing cardiovascular disease in the medical field as there has not been sufficient validation studies of the proposed methods presented by researchers. The goal of this study is to validate the neural network that is trained using simulated blood pressure and flow data to predict aortic systolic and diastolic diameters with clinical data and blood pressure waveforms through the use of MATLAB software. Numerical models are performed on the clinical blood pressure waveforms to estimate the flow and arterial compliance corresponding to the given systolic and diastolic blood pressures. Arterial compliance values are then inputted into the neural network, and the targets provide the systolic and diastolic aorta diameter predictions. The preliminary validation testing results based on human clinical data are discussed and reviewed against published clinical data on aortic diameters.

Table of Contents

List of Figures

Acknowledgement

Completion of a master's degree in Biomedical Engineering as well as authoring a thesis in one short year has be an incredibly rewarding accomplishment in my life. There is no way that I would have been able to do this without the overwhelming amount of support that I have had not only this year, but throughout my entire academic life.

First and foremost, I would like to thank Dr. Mehmet Kaya for welcoming me into his lab during my Sophomore year of college when I had no previous research experience but was eager to start learning. From getting to assist on blood pressure related clinical trials to learning about computational modeling of the cardiovascular system, Dr. Kaya has been there to mentor and guide me over the past five years.

Additionally, I could not have gotten to where I am without guidance from Vignesh and the other BME graduate students who have consistently helped me grow as a biomedical engineer.

Finally, I would like to thank my family: Kris, Gary, Alex, Tiffanie, Ally, Rita, and LaVerne. I would also like to thank my boyfriend, John. With the help of their unconditional love and support day in and day out, I have been able to reach this incredible point in my career.

Dedication

I would like to dedicate this thesis to my parents: Kris and Gary. Without their love and support throughout my entire life I would not be in a position to be graduating with my master's degree in Biomedical Engineering during a global pandemic. Thank you for not only believing in me but teaching me over the years to believe in myself. Without you guys, I would not be the person I am today if I had not been blessed with such loving parents. I love you both so much. This is for you.

Chapter 1
Introduction

1.1 Motivation

Cardiovascular diseases (CVD), specifically heart disease, is the leading cause of deaths worldwide as it accounts for one out of every four deaths (*World Health Organization* 2020). CVD is even more prevalent in American women as heart disease accounts for 1 in 3 deaths (Garcia et al. 2016). The Center for Disease Control and Prevention (CDC) reported as of 2018 that every 36 seconds, someone in the United States will be killed by a cardiovascular disease (*The Center for Disease Control* 2020). In 2016, 17.6 million people died from CVD alone, with a 14.6 percent increase in deaths as seen in comparison to data from 2006 (Benjamin et al. 2019). The most alarming finding regarding CVDs in the United States is that not only the life expectancy has stalled, but if there are not advances in preventing CVD mortalities in the near future, the life expectancy will begin to decline (Mehta et al. 2020).

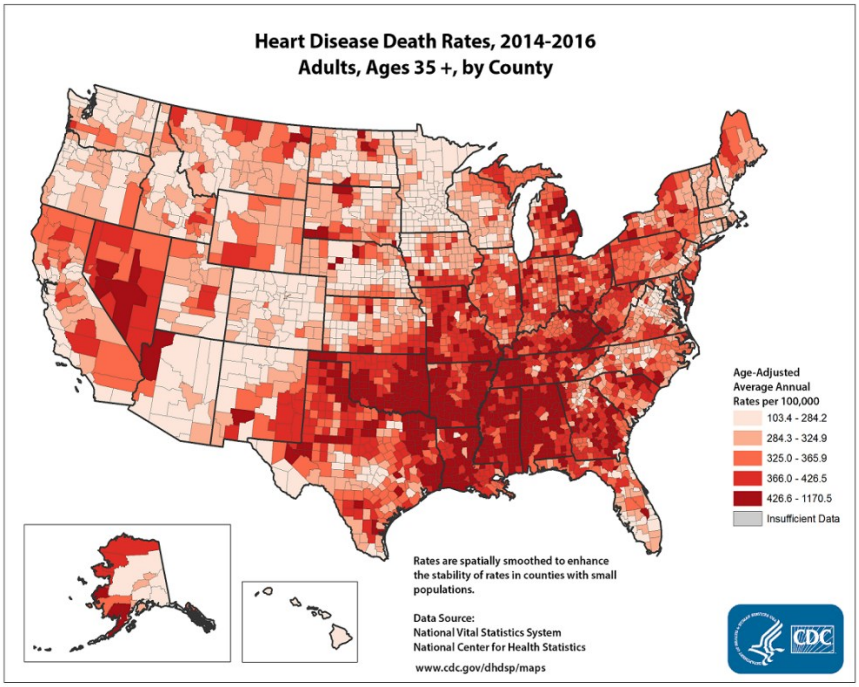

Figure 1: Map of deaths due to heart disease in the United States between 2014 to 2016 (*The Center for Disease Control and Prevention,* 2019)

The CDC released an interactive map, seen by Figure 1, to allow people to see how prevalent heart diseases are here in the United States as there is an alarming increase in deaths in Americans over 35 years old from 2014 to 2016, with statistics showing that these numbers are still increasing now in 2021.

Computational fluid dynamics (CFD) is tough to model in the biomedical engineering field as the human body fluid behaviors are highly complex, especially the cardiovascular system (Lee 2011). This methodology allows for both researchers and physicians to better understand the human body fluid dynamics as well as to use this information to determine treatment and prevention for progression of diseases.

The cardiovascular system is a vast area of research in the medical field as it is crucial to slow down the mortality rates for CVDs worldwide. It is necessary to use pre-processing, mathematical equations, and post-processing to create CFD models on a computer regardless of the engineering discipline the model is being developed for (Lee 2011). Limitations that have been noticed by many researchers include the lack of access to clinical databases that provide all the necessary information from the patient's cardiovascular system such as diameter measurements, blood pressure waveforms, and raw variable data as many only publish using mean values observed. This makes it difficult to both accurately create a model and further the research to predict aortic diameters as the neural network requires a large complete database to be trained to the accuracy desired for use in clinical settings.

With more sophisticated software and advances in computer science, it is now possible to make meaningful advances in CFD technologies for the human body. One main concern throughout the medical community is with the increasing amount of CFD models being published for predicting CVD risks since there is a vast need to validate these models before it can be decided there is a clear benefit in funding the future research for these models (Damen et al. 2016). This concern in the medical community is why this validation study was crucial to show the promising potential of this aortic diameter prediction to be utilized in the medical field to determine CVD risk.

1.2 Background

Heart disease is a type of disease that will affect the heart structure and function, while CVD is any type of disease that will affect the heart or blood vessels (Gaziano & Manson 1996). The most common known cause of CVD is atherosclerosis, the buildup of fatty plaque in arteries (*The Center for Disease Control and Prevention,* 2021). Risk factors that influence risk of developing a cardiovascular disease are smoking, being diagnosed with diabetes mellitus, exhibiting signs of hypertension or dyslipidemia, being physically inactive, and being obese (Garcia et al. 2016).

The American Heart Association (AHA) predicts that by 2030, 40.5% of the United States population will suffer from one type of CVD, costing the healthcare system approximately 1 trillion dollars per year (Tomaselli et al. 2011). The AHA committee made their 2020 Health Impact Goal to improve cardiovascular health and reduce CVD mortality risk by 20 percent (Lloyd-Jones et al. 2010). It is crucial for one to understand their CVD risk better to help prolong their life. Researchers and physicians are working hard to better understand trends in CVD mortality and risks to aid in the diagnosing and treatment of these heart diseases before they cause detrimental damage to their cardiovascular system (Wilson et al. 2017). To help improve determining an individual's CVD risk, it is crucial to further development

into obtaining more accurate information from non-invasive measurements as many individuals do not have access to preventative healthcare measures to have invasive procedures performed in hospital settings.

With an ongoing global pandemic due to SARS-CoV-2, there is an even larger demand than ever before for non-invasive ways to measure one's cardiovascular baselines. It is prevalent for cardiovascular baselines to be determined as this virus has proven to not only attack the respiratory systems of those affected but many other organs as well, including the heart (Bansal 2020). This is largely due to the fact that the viral spike protein binds to human angiotensin-converting enzyme 2 receptor which is largely expressed in the heart, lungs, intestinal epithelium, vascular endothelium, and kidneys (Clerkin et al. 2020). A study in Germany showed that the SARS-Cov-2 virus primary target and secondary co-morbidity factor for the three progression phases is the cardiovascular system, with the heart itself being a direct target for the viral infection (Böhm et al. 2020). Also, the risk of developing a severe case of the SARS-CoV-2 virus if one already has an underlying CVD is much higher and accounts for 40 percent of the COVID-19 deaths in hospitals (Bae et al. 2021).

1.3 Feedforward Neural Networks

Neural networks are computational learning systems that utilize a collection of functions to understand inputs and then translate the information into desired outputs of another form. A feedforward neural network is the simplest type of neural network as it moves information in a forward unidirectional flow from the inputs to obtain the desired output (Schmidhuber 2015).

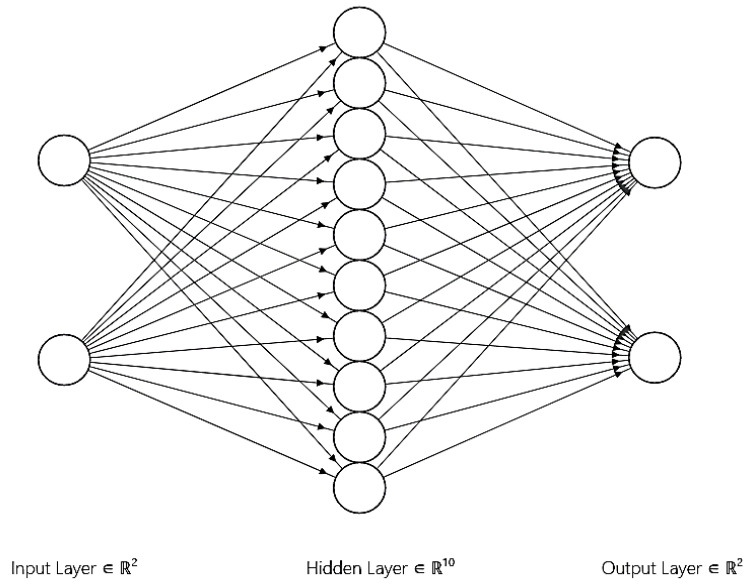

Figure 2: Feedforward neural network architecture

A feedforward neural network will feed inputs into input layers which then lead to hidden layers and finally go through output layers to yield the predicted outputs. The input layer is where the inputs are received, the hidden layer is where the relationships between the inputs and outputs can be determined, and the output

layer is where the outputs of the neural network are computed (Dongare et al. 2012). There are also neuron weights that demonstrate the strength of the connection between two of the neurons, often ranging between 0 to 1. The activation function is utilized in the hidden and output layers to map the summed weighted input to the output of the neurons (Dongare et al. 2012). Activation functions will govern the initiation of neurons to be activated to impact the strength of the predicted output.

The neural network utilized for this thesis has 1 input layer containing 2 neurons, 1 hidden layer containing 10 neurons, and 1 output layer containing 2 neurons which can be seen in Figure 2. The 10 hidden neurons are 10 different 1^{st}-order polynomial equations for the input and outputs and are used to obtain multiple representations of arterial compliance predictions prior to giving the predicted aortic diameters. Further details of the neural network will be discussed in the following section.

The neural network computes data in 4 simple steps: multiplying the weights and inputs, adding in the biases, performing activation functions, and obtaining the output signal. The inputs first get multiplied by the assigned weights. Next, the temporary products found from the input layer is added to the respective biases to produce the next temporary product. After the temporary product is created the activation functions are utilized to rescale the products and turn the weighted sum into the output signals.

1.4 Blood Pressure Waveform

Blood pressure (BP) plays a significant role in determining CVD risk in patients and is a major contributing factor during cardiovascular events (Asia Pacific Cohort Studies 2003). Blood pressure is the pressure exerted on the artery by the blood as it moves through the body. The two main values observed in blood pressure are the systolic and diastolic blood pressures. Systolic blood pressure (SBP) is the pressure in the artery when the heart beats, while diastolic blood pressure (DBP) is the pressure in the artery when the heart rests. Historically, diastolic blood pressure was initially thought to have a stronger correlation with CVD risk as this was seen in earlier clinical trials, but more recently research has shifted to show that systolic blood pressure is actually a better indicator for CVD risk (Kengne et al. 2009).

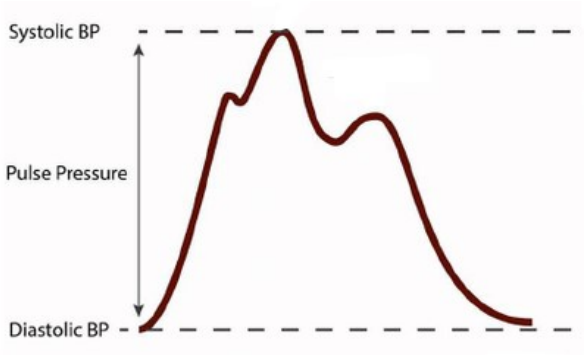

Figure 3: Aortic pressure waveform of a healthy, normotensive subject (Van Varik et al. 2012)

The simplified, normal aortic blood pressure waveform of a human is seen in Figure 3. The waveform begins with the onset, which is the initiation of the pressure

waveform on the left most portion of the wave. The first peak seen to the left is the inflection point, which is crucial for determining the compliance of the aorta (Segers et al. 2007). The next peak to the right is the systolic peak and is clearly indicated by the highest point in the waveform. The final peak on the pressure waveform is the diastolic peak. In between the systolic and diastolic peaks is a downward notch, this notch is known as the dicrotic notch.

The standard blood pressure for a normal, healthy adult is approximately less than or equal to 120 over 80 millimeters of mercury (mmHg), where 120 mmHg is the systolic blood pressure and 80 is the diastolic blood pressure (Staessen et al. 2017). Fluctuations in blood pressure can be caused by variables such as genetic predispositions to hypertension, advancing age, increased sodium intake, sleep apnea, consumption of alcohol, and mental stress (Oparil et al. 2018).

1.5 Inflection Point

The inflection point is an indicator of arterial stiffness in blood vessels and is seen by the leftmost peak in the blood pressure waveform (Narayan et al. 2013). As the inflection point is clearly visible in healthy, normotensive humans, it is an important indicator of potential CVDs if the waveform does not clearly depict this point or peak. If a blood pressure waveform has an inflection point that arrives earlier

and in a shorter amount of time than normal, the person either has atherosclerosis or another CVD that affects the diameter of the arteries.

1.6 Three-Element Windkessel Model

The Three-Element Windkessel model, created by Frank Windkessel, can be used to estimate the total arterial compliance from non-linear blood pressure and flow in one lumped model (Westerhof et al. 2009). The Windkessel effect is widely accepted for use in the medical field to model the shape of the arterial blood pressure waveform, in this case the aorta.

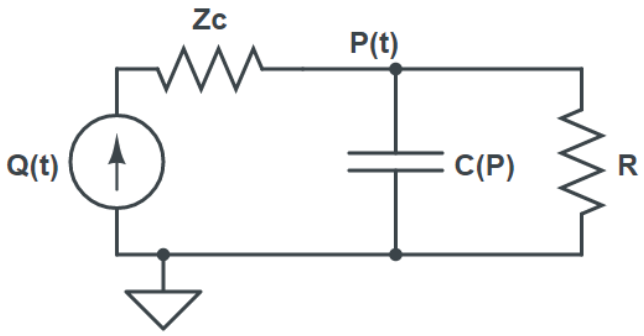

Figure 4: Three-Element Windkessel Model developed by Westerhof

As seen by Figure 4, Q(t) represents the blood flow, Zc is the characteristic impedance, P(t) is the aortic blood pressure, C(P) is arterial compliance, and R is the peripheral resistance. The Three-Element Windkessel model has C(P) and R in a parallel arrangement with Zc in series with them.

The governing equation for the given Three-Element Windkessel model by Westerhof is:

$$P(t) + [R*C(P)] * \frac{dP(t)}{dt} = (R + Zc) * Q(t) + [Zc*R*C(P)] * \frac{dQ(t)}{dt} \quad (1)$$

To utilize this model, it is necessary to obtain the values of the stroke volume, compliance, characteristic impedance, and peripheral resistance values from the aorta. This model assumes that the compliance of the aorta can be modeled as a continuous, steady flow regardless of the heart being in systole or diastole (Kaya et al. 2018).

1.7 Arterial Compliance and Distensibility

Clinical studies have shown that arterial compliance is associated with, one of the most common CVD, hypertension which shows that there is a clinical need to know this value when determining one's risk of developing hypertension or any other CVD (Kaya et al. 2018). Arterial compliance is defined as the change in the geometry of the arteries in relation to a change in blood pressure, while the arterial distensibility is the fractional change in artery area in relations to a change in blood pressure (Glasser et al. 1997).

Arterial compliance is inversely related to vascular stiffness. If a person is of advanced age, has atherosclerosis formation, and other CVDs their compliance will decrease. Arterial distensibility allows for stress on the arterial wall to be determined. If there is a decrease in distensibility, the arterial wall is at risk of damage. Monitoring changes in compliance and distensibility is crucial in the prevention and treatment of life-threatening cardiovascular events that can stem from CVDs.

1.8 Clinical Importance of Aortic Diameter

The diameter of the aorta is larger in men than women and will increase as the person ages (Mao et al. 2009). Research has shown that the widening of the aorta has been linked to numerous CVD risk factors and may increase the risk of the patient undergoing cardiovascular events (Qazi et al. 2017, Laughlin et al. 2011, Chuang et al. 2018). The pressure-diameter changes in the human aorta are non-linear so larger changes are expected to occur at decreased pressures, while smaller changes are expected during increased pressures (Murgo et al. 1981). These results depict that the change in the aortic diameter can be a promising factor for determining their risk of developing a CVD in the future. Patients with dilated, larger diameters than the normal range, aortas have been linked to be at a higher risk of developing CVDs than those who exhibit less dilation (Paul et al. 2020).

The average aorta systolic and diastolic diameters for healthy, normotensive adults 18 to 75 was observed to be between 16 to 23 and 15 to 22 cm respectively (Länne et al. 1992, Stefanadis et al. 1995). These findings agree with the cardiovascular physiology as the systolic diameter of the aorta should always be larger than the diastolic diameter of the aorta. As this study aims to observe the aorta systolic and diastolic diameters, it can be concluded that the predicted diameters must be no smaller than 15 cm and no larger than 23 cm to remain physiologically possible in the adult human aorta.

1.9 Project Scope

It is more important than ever before to strive to continue advances towards non-invasive cardiovascular medical devices to allow for fast, low cost, and accurate monitoring of CVD risk throughout their life. By creating a new method for predicting aortic diameters, it will allow for easier evaluation of changes in the cardiovascular system non-invasively. This will allow for physicians to more effectively monitor those who may be at an increased risk of developing CVD. Physicians will also be able to continue to make advances in preventing those with low to moderate risk of developing CVD to stay under control for a longer time without the need for medical interventions. Ultimately this predictive software could be utilized by physicians in an outpatient, clinical setting which could reduce the

financial burden posed to patients to undergo invasive cardiac procedures for diagnosis of CVDs in the future.

Currently, there is no non-invasive, low-cost, or fast way to measure aortic diameters in an average clinical setting. The only way to measure aortic diameters would be to undergo a non-invasive procedure in a hospital setting, which can be extremely costly. Creating a non-invasive way to predict aortic diameters will not only save patients time and money, but help physicians create a baseline for their patients so that they can monitor changes in their patient's cardiovascular system to help prevent them from developing CVDs that can shorten their life expectancy significantly.

Chapter 2
Materials and Methods

2.1 Experimental Overview

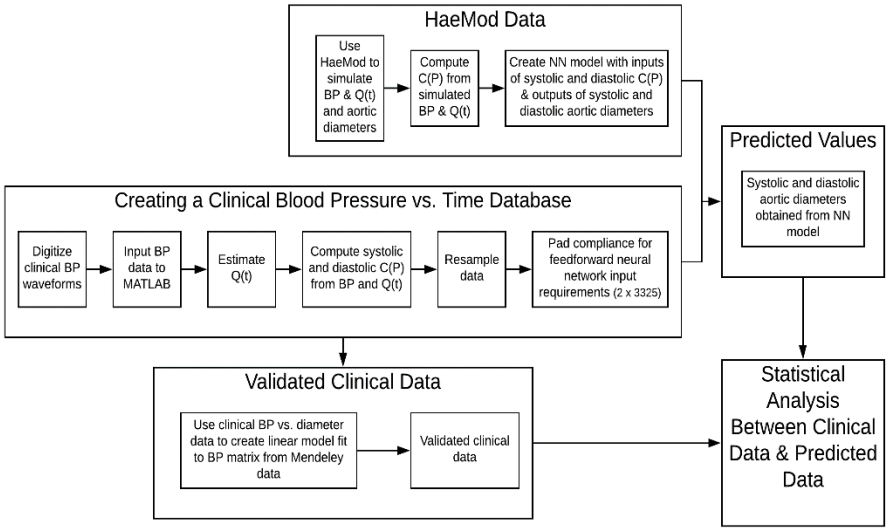

Figure 5: Brief flow chart of experiment

The overall experimental process is depicted by Figure 5. The details of the experimental steps are explained in the following subsections.

2.2 Creating a Clinical Blood Pressure vs. Time Database

2.2.1 Mendeley Clinical Blood Pressure vs. Time Waveform Collection

Clinical data was sought out to build a database of continuous arterial pressure data using Mendeley to aid in finding arterial blood pressure waveforms to

digitize. Mendeley is a free tool that is accessible on the web that helps researchers organize and collect research articles for academic research purposes (Holt et al. 2011). 37 blood pressure versus time waveform plots of healthy, normotensive human subjects were collected for re-digitization through the use of Mendeley to create a database for the validation study. Mendeley allowed for the 37 clinical blood pressure plots from healthy human subjects to be found quickly from 17 reference articles by searching the online database for central aortic pressure waveforms.

The first blood pressure waveform was collected from the Williams *et al.* paper. The second and third reference papers both provided 4 waveforms to be collected for digitization (O'Rourke & Adji 2008, Nichols 2005). The fourth reference paper collected from Mendeley provided 2 blood pressure waveforms for use in digitization (O'Rourke & Seward 2006). A fifth article provided 6 waveforms for digitization (O'Rourke & Hashimoto 2007). The sixth and seventh references both provided one useful waveform for digitization (Nichols et al. 2013, Smith et al. 2004). The eighth reference paper provided 2 more blood pressure waveforms for creating the database (Lowe et al. 2009). The ninth article, written by Townsend *et al.* in 2016, provided 3 additional waveforms for digitization and the tenth reference paper by Elvan-Taşpinar et al. yielded one additional waveform. An eleventh and twelfth reference article gave 2 and 4 waveforms respectively for the database construction (Lim et al. 2009, Afzal et al. 2014). The thirteenth through sixteenth

reference papers all yielded 1 additional blood pressure waveform to the database (Subherwal et al. 2010, Matthys et al. 2007, Hrušková et al. 2015, Townsend et al. 2015). The last reference article, written by Tomoaki Murakami, provided the final 2 blood pressure waveforms needed to complete the database for the validation study.

2.2.2 Digitizing Blood Pressure Waveforms

After collecting the 37 datasets, the WebPlotDigitizer version 4.4 tool available by automeris.io was used to create the database of pressure and time data for each waveform graph. The WebPlotDigitizer is a free, online software that allows researchers to reverse engineer images to extract the numerical data that is necessary for conducting research studies (Marin et al 2017).

The WebPlotDigitizer tool allowed for time and pressure data to be collected via the use of the scatter plot tool for the validation study. This software allowed for the clinical database to be constructed with numerical time and blood pressure data prior to being run through the MATLAB code necessary for the aorta diameter prediction modeling. To utilize this tool, the waveforms axes needed to be clearly identified and labeled. Figure 6 depicts how the WebPlotDigitizer tool was utilized to extract the tabular pressure and time data for the given clinical blood pressure waveform.

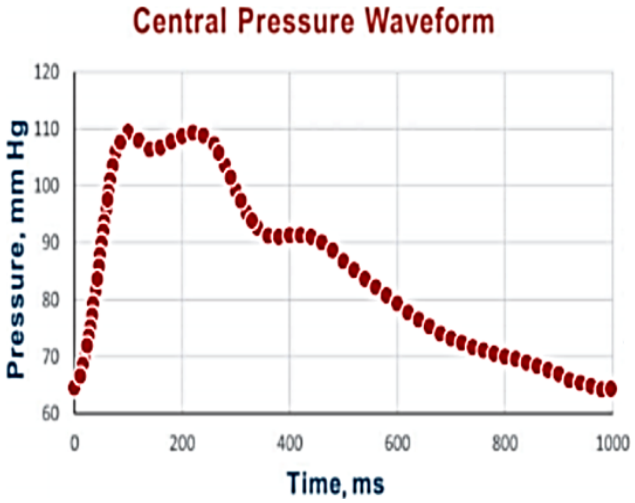

Figure 6: Example of Digitizing a Blood Pressure Waveform Using the WebPlotDigitizer Tool

To utilize the MATLAB code, the pressure needs to be mmHg. The one waveform collected had pressure in kilopascals (KPa) would first need to be converted into mmHg once digitizing occurred to accurately predict the normalized flow and compliance for the neural network. The data also needed to be collected in seconds, thus all the waveforms in milliseconds (ms) needed to be converted into seconds after digitization as well.

2.2.3 Computation of Blood Flow From Blood Pressure

Blood flow data from the aorta needed to be estimated as the database created did not have this information readily available. Westerhof *et al.* published a study that allows for wave reflection to be determined from uncalibrated blood pressure

alone, allowing for blood flow in the aorta to be estimated. Blood flow data is necessary to calculate arterial compliance as without flow in the aorta there would be no change in diameter or movement of blood being observed.

Waveform separation analysis is the gold standard for assessing wave reflections in the heart (Segers et al. 2007). The waveform analysis is performed by breaking down the blood pressure waveform into its forward and backward pressures. A normalized flow method was utilized based on the findings of Westerhof *et. al* to calculate human aorta wave reflection through the use of assuming a triangular shaped flow wave as well as the actual measured blood pressure (Westerhof et al. 2006).

By manipulating the governing equation of the Three-Element Windkessel model, as seen in equation 1, the unknowns needed to estimate blood flow and arterial compliance from the given blood pressure waveforms can be calculated.

The peripheral resistance of the Three-Element Windkessel model is calculated using the equation:

$$R = \frac{Mean\ (\ P(t)\ )}{Mean\ (\ Q(t)\ )} \tag{2}$$

Peripheral resistance must be found to depict the resistance of blood flow through the aortic artery given the blood pressure waveform. The peripheral resistance calculated using equation 2 allows for the characteristic impedance to now

be found from the frequency domain. This furthers the process needed to obtain the aortic blood flow, as it is impossible to determine the arterial compliance in the aorta without it.

The characteristic impedance of the Three-Element Windkessel model is also able to be calculated using the equation:

$$Zc = \left|\frac{P(t)}{Q(t)}\right| \quad (3)$$

After the characteristic impedances are found for the waveform using equation 3, additional coding manipulation is performed to obtain the maximum value for Zc that is not an outlier by using the MATLAB built in functions “mean” and “isoutlier”.

Once the maximum characteristic impedance is found for the waveform, the aortic blood flow can be calculated using the equation:

$$Q_a(t) = P(t) - Zc * Q(t) \quad (4)$$

The aortic blood flow found using equation 4 is necessary to calculate the arterial compliance of the blood pressure waveform. Arterial compliance requires blood flow as the artery will not distend if there is no blood pumping through it.

The inflection point was calculated in regard to the pressure by the equation:

$$I(t) = \frac{d^2P(t)}{dt^2} \quad (5)$$

The shoulder point was then calculated in regard to the inflection point by the equation:

$$S(t) = \frac{d^2I(t)}{dt^2} \quad (6)$$

To ensure that the timing of the reflected waves from the pressure waveform analysis agree, the inflection point, seen by equation 5, and shoulder point, seen by equation 6, need to be verified to match when transposed on each other. The inflection and shoulder points correspond to the automated algorithm when the second derivative and fourth derivative crosses zero on the x-axis respectively (Segers et al. 2007). These characteristic points on the waveform are found using the MATLAB built in function “gradient”.

The upward slope of the flow wave is found by taking the time derivative of the blood pressure waveform and multiplying it by the time required to reach the median between the inflection and shoulder points. This will allow for the derivative of the blood pressure slope to be taken from the onset to the systolic peak to give the forward flow of the aorta.

The downward slope of the flow wave is found by taking the negative time derivative and multiplying it by the time required to go from the shoulder point, the diastolic peak to the offset of the blood pressure wave and subtracting the time

required to hit the shoulder point. This will allow for the derivative of the blood pressure downward slope to give the backward flow of the aorta.

2.2.4 Computation of Arterial Compliance From Blood Pressure and Blood Flow

The digitized data is then run through MATLAB to compute the arterial compliance as seen in the Kaya *et. al* paper based on the findings of a compliance-pressure loop (Kaya et al. 2018). This compliance-pressure loop utilizes the Three-Element Windkessel model as well as compliance to display how compliance affects the diameter and blood pressure of the aorta.

This method can be utilized now as the database made now has pressure and generated flow data.

Arterial compliance is computed using the following equation:

$$C(P) = ae^{b*P(t)} \tag{7}$$

C(P) is the arterial compliance, a and b are constants defined by the Windkessel model, and P(t) is the aortic pressure (Li & Zhu 1994). The constants a and b are the numerical solutions to equation 1 and indicate where the root mean square error between the actual pressure and the predicted pressure are minimized.

Equation 7 allows for arterial blood pressure compliance to be modeled as a nonlinear pressure dependent element of the aorta. This computation of arterial compliance allows for the stiffening of arteries to be accounted for while it is under pressure to better represent the normal cardiovascular physiology.

2.2.5 Resampling and Padding Arterial Compliance Data

Compliance is calculated for each waveform in the database and then put into an array for use in the neural network. The arterial compliance, pressure, and time are then resampled to 1000Hz using the built in MATLAB "interpl" to be compatible with the neural network requirements. The arterial compliance data then needed to be padded to a [2 x 3325] matrix size to satisfy the input size requirements for the neural network.

2.3 Creating a Neural Network Model From HaeMod Group

2.3.1 Simulate Blood Pressure, Blood Flow, and Aortic Diameters

The Deep Learning Toolbox in MATLAB was utilized to train a simple feedforward neural network to predict the systolic and diastolic aortic diameters. A feedforward neural network is the simplest type of artificial neural network as the information only moves in one direction from the input (Schmidhuber 2015).

This neural network, seen in Figure 2, was created using simulated blood pressure, blood flow, and cross-sectional area data from the open sourced HaeMod database created by the HaeMod Group (Willemet et al. 2015).

The cross-sectional area data from the HaeMod Group is converted into aortic diameters using equation 8.

$$A = \pi r^2 \tag{8}$$

The trained feedforward neural network was then utilized to predict the aortic systolic and diastolic diameters given the blood pressure data collected in the clinical database.

2.3.2 Creating Neural Network Model Input and Outputs

The inputs for the neural network accept data in the size of 2 by N double array. N refers to the number of test datasets. The neural network uses the computed arterial compliance data as the input. The first input corresponds to the systolic arterial compliance and the second input corresponds to the diastolic arterial compliance. The units for the input are 1/mmHg.

The outputs, or targets, for the neural network give data in the size of 2 by N as well. The first output corresponds to the systolic aortic diameter and the second

output corresponds to the diastolic aortic diameter, respectively. The units for the output diameters are meters (m).

The feedforward neural network is executed using a variety of weights and functions. The input layer weights are a [10 x 2] matrix with the first column being the systolic weights and the second column being the diastolic weights. The hidden layer weights are a [2 x 10] matrix with the first row being the input systolic weights and the second row being the input diastolic weights.

The first step of the neural network is to perform element by element multiplication of the input weights by the input systolic and diastolic arterial compliances computed for the waveforms in the database. This is seen by equation 9. This equation is then repeated for the remaining 9 pairs of weights by changing the 1 in the IW portion for each pair i.e. (IW(2, :). * C(P)(1, :) for the second pair).

$$IW(1, :). * C(P)(1, :) = Temporary\_product\_0 \quad (9)$$

The second step is to add the first bias, a [10 x 1] matrix, to the temporary_product_0 found in equation 9 to compute the temporary product from the input layer of the neural network. This is seen in equation 10.

$$Temporary\_product\_1 = Temporary\_product\_0 + bias\_1 \quad (10)$$

After the temporary product from the input layer is computed it is run through the first activation sigmoid equation to gives the value between the first and second

temporary products to rescale Temporary_product_1 without changing the overall size of the matrix. The sigmoid equation used in the input layer is seen in equation 11.

$$\text{Temporary\_product} = \frac{1}{1+ exp^{-temporary\_product\_1}} \tag{11}$$

The third step of the neural network is to multiply the hidden layer weights by the temporary products from the input layer. This is performed by equation 12 for the systolic predictions and equation 13 for the diastolic predictions.

$$\text{Temporary\_product\_2\_1} = \text{LW}(1, :). * \text{Temporary\_product}(: , 1) \tag{12}$$

$$\text{Temporary\_product\_2\_2} = \text{LW}(2, :). * \text{Temporary\_product}(:, 2) \tag{13}$$

The fourth step is to add the hidden layer bias or second bias to each result from the hidden layer to produce the initial outputs. The second bias is a [2 x 1] matrix. This is seen in equation 14 for the systolic diameter outputs and equation 15 for the diastolic diameter outputs.

$$\text{Systolic\_outputs} = \text{Temporary\_product\_2\_1} + \text{bias\_2}(1) \tag{14}$$

$$\text{Diastolic\_outputs} = \text{Temporary\_product\_2\_2} + \text{bias\_2}(2) \tag{15}$$

The fifth step of the neural network in this case is to apply the activation function for the hidden layer, which in this case is a linear function, thus the value does not change as seen in equation 16.

Linear equation: y = x (16)

As there were no changes with the activation function, the neural network is now completed. This will allow for the predicted systolic and diastolic diameters to be computed.

The neural network training, validation, and testing were sampled at 50, 20, and 30 percent respectively for a total of 3,325 samples.

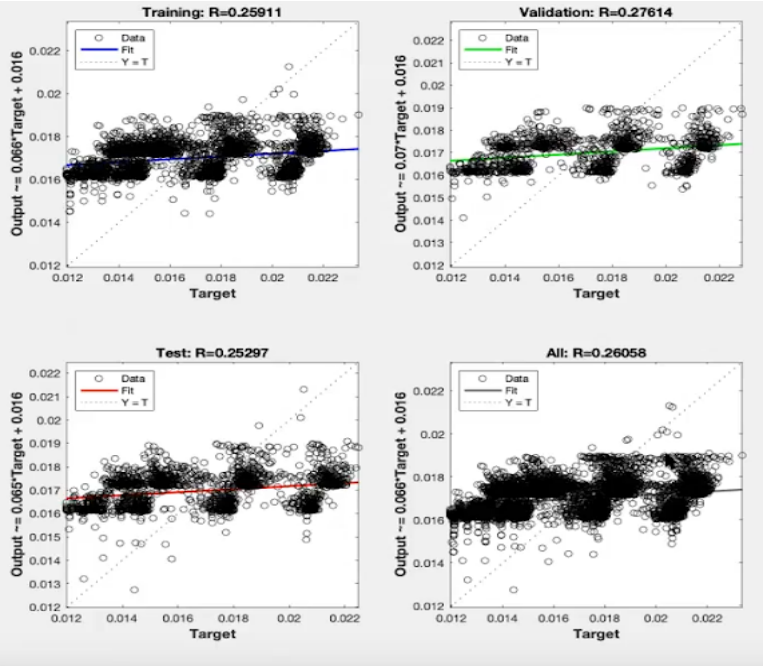

Figure 7: Regression Plots From Neural Network Model

The neural network yielded a mean squared error (MSE) of 7.55820e-6, 7.51369e-6, and 7.69041e-6 for the training, validation, and testing, respectively. The extremely small MSE means that at least the first 2 decimals are correctly

predicted. The R value for training data was 2.59110e-1, for validation data was 2.76139e-1, and for testing data was 2.52969e-1, which can be seen by Figure 7. This depicts that there is not much correlation as the predictions are non-linear, which is expected as the cardiovascular system is not a linear function.

2.4 Validated Clinical Data

A simple linear model was created using validation studies of clinical data by taking in both the systolic pressure and diastolic pressure to predict the aortic systolic and diastolic diameters, respectively.

To utilize the clinical data, digitization of the arterial pressure was performed using the blob detector and line detection functions in the WebPlotDigitizer, seen in Figure 8.

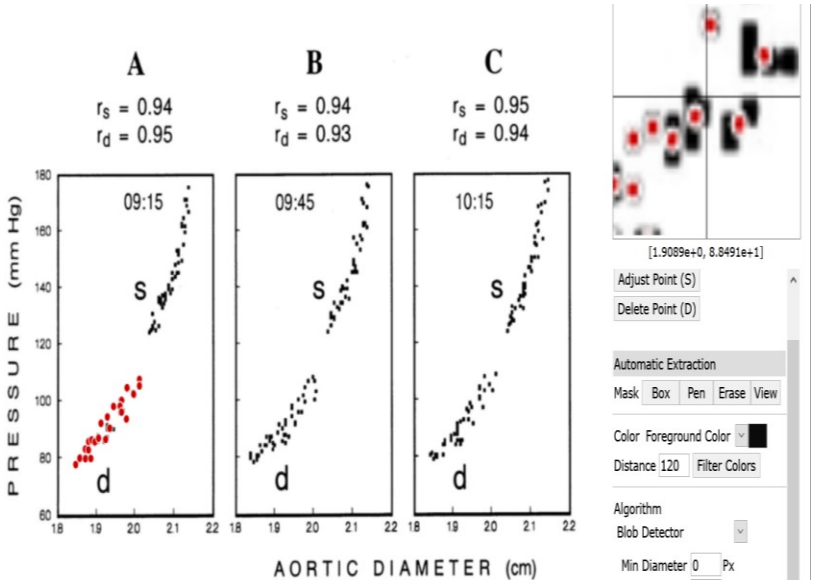

Figure 8: Example of Using the WebPlotDigitizer Blob Detector Tool to Digitize the Clinical Arterial Blood Pressure vs. Aortic Diameter Data

Once the clinical data was digitized the MATLAB built in function "fitlm" will be utilized to return a linear regression model of the responses of diameter data, fit to the data matrix of blood pressure collected from the clinical database.

For the first study, a simple linear model is generated from the clinical data reported by Stefanadis *et. al* for both systolic and diastolic blood pressure (Stefanadis et al. 1995). In the second validation paper by Länne *et. al*, the linear model will take in average aorta blood pressure and then be used to predict the systolic and diastolic diameters respectively, as the reference study did not separate the mean pressures observed in the age groups by systolic and diastolic pressure but rather as just blood pressure in general (Länne et al. 1992).

2.5 Statistical Analysis Between Clinical Data and Predicted Data

Results are collected to compare the validation study diameters against the predicted neural network diameters to determine if the neural network performs well at predicting the systolic and diastolic arterial diameters or not. This was performed by using built in MATLAB functions to perform correlation analysis, normality tests, Kruskal-Wallis ANOVA analysis as well as excel to perform Bland-Altman analysis of the data.

The correlation analysis was performed using the MATLAB function “corr” with the spearman correlation specified as the cardiovascular system is non-linear. Correlation analysis was conducted to determine if the neural network predicted aortic diameters that were strongly related to the reference validation aortic diameters observed.

To determine which type of ANOVA test could be performed on the predicted systolic and diastolic diameter model data, normality plots were to be constructed and analyzed again. If the population is normally distributed, then the one-way ANOVA test is utilized, if the population is non-normally distributed then the Kruskal-Wallis test is necessary. The one-way ANOVA is performed using the MATLAB function “anova1” and the Kruskal-Wallis ANOVA is performed using the MATLAB function “kruskalwallis”. The p-value of the ANOVA would allow

for one to determine if the null hypothesis should be rejected or not as it will show the probability of getting a result as extreme as the one observed in the plot (Hecke 2011).

The normality tests were performed using the MATLAB function “histfit” with the normal distribution. This allowed for the normal density function to be fitted to the data to see if the data collected was from a normal or non-normal population based on the presence of a bell curve or skewed curve being observed in the histogram.

The Bland Altman Analysis was used to show the agreement between the reference validation aortic diameters and the neural network predicted aortic diameters. Bland Altman Analysis plots are the simplest way to evaluate bias in the mean differences as well as estimate the 95 percent agreement interval between two quantitative methods of measurement (Giavarina 2015). The actual Bland Altman Analysis plot will depict the difference between the paired measurements on the y-axis and the average of the two measurements on the x-axis. Giavarina explains that a Bland Altman Analysis plot should contain at least 95 percent of the data points within ±2 standard deviations.

Chapter 3
Results and Discussion

3.1 Neural Network Reference Data Results

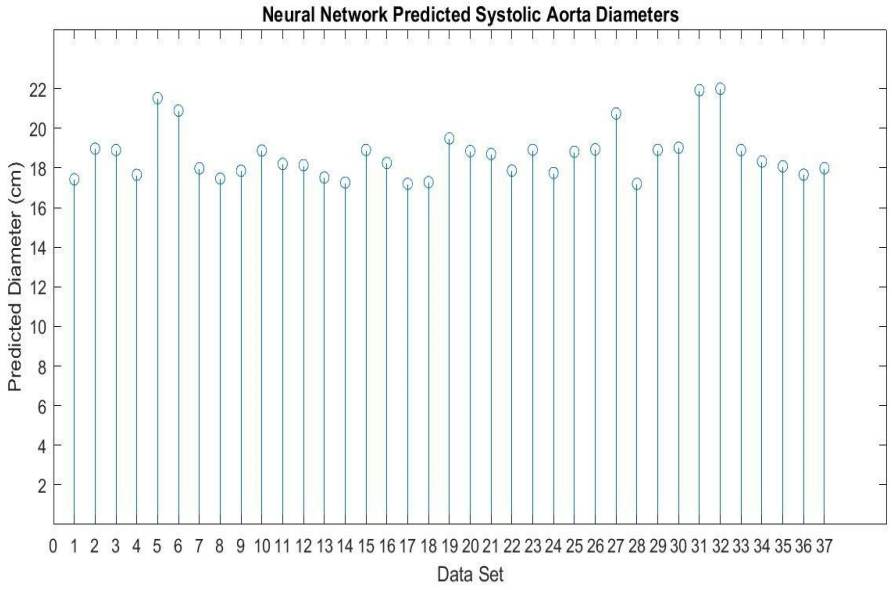

Figure 9: Stem plot of the neural network predicted systolic aortic diameter for each reference data set

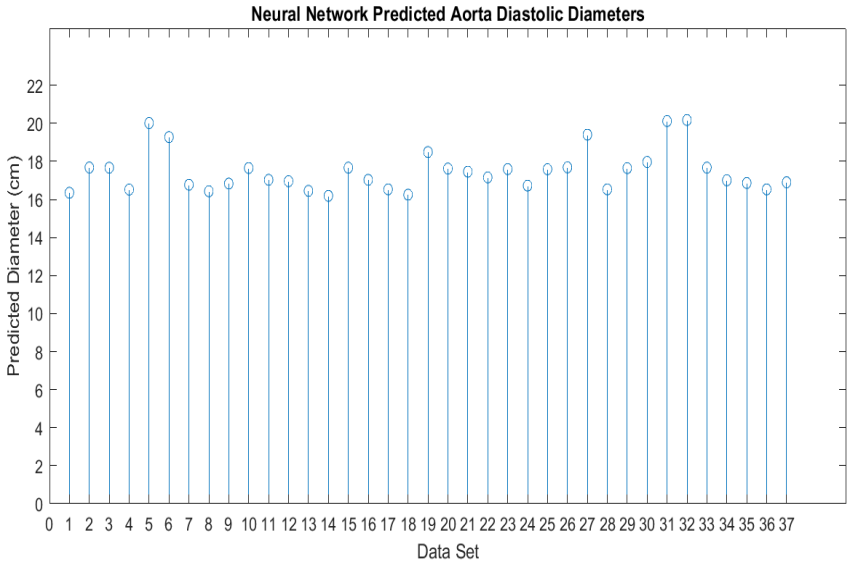

Figure 10: Stem plot of the neural network predicted diastolic aortic diameter for each reference data set

Figure 9 andFigure 10 show that the neural network predicted the aorta systolic diameters to fall between 17 to 22 cm and the aorta diastolic diameters fall between 16 to 20 cm respectively. These values fall within the normal range of aorta diameters seen in healthy adults. The mean systolic diameter and pressure predicted by the neural network was 19.23 cm at 91.94 mmHg. The mean diastolic diameter and pressure predicted by the neural network was at 20.09 cm and 146.31 mmHg.

3.2 First Validation Study Trial 1 Results

The following results will be based on the findings of the research article, by Stefandis *et al.*, “Pressure-Diameter Relation of the Human Aorta”.

Predicted Diameter Linear Models based on figure 5 in the Stefanadis *et. al* paper of the A, B, C graphs of pressure versus aortic diameter at different regression values for the systolic and diastolic diameters, respectively. The graphs are of the diameter and pressure values observed in a subject at 09:15 for Graph A, 09:45 for Graph B, and 10:15 for Graph C. Each Graph has the correlation values for the systolic and diastolic diameters given above the graphs as well.

The linear models were found using the MATLAB function "fitlm".

$$\text{Systolic Model A: } y = 2.0201e\text{-}05x + 0.017977 \quad (17)$$

$$\text{Diastolic Model A: } y = 5.1121e\text{-}05x + 0.014568 \quad (18)$$

For graph A, at regression values of 0.94 and 0.95, the systolic linear model created is seen by equation 17 and the diastolic linear model created is seen by equation 18. The systolic model has a mean squared error (MSE) of 1.0650e-08 and a R^2 value of 0.8882. The diastolic model for graph A had an MSE of 2.2196e-08 and R^2 value 0.9052.

$$\text{Systolic Model B: } y = 2.0772e\text{-}05x + 0.01785 \quad (19)$$

$$\text{Diastolic Model B: } y = 5.3986e\text{-}05x + 0.014268 \quad (20)$$

For graph B, at regression values of 0.94 and 0.93, the systolic linear model created is seen by equation 19 and the diastolic linear model created is seen by

equation 20 .The systolic model yielded a MSE of 1.2096e-08 and R^2 value of .8909. The diastolic model for graph B yielded a MSE of 3.794e-08 and R^2 value of .08722.

$$\text{Systolic Model C: } y = 1.8552e\text{-}05x + 0.018205 \quad (21)$$

$$\text{Diastolic Model C: } y = 4.7161e\text{-}05x + 0.014877 \quad (22)$$

For graph C, at regression values of 0.95 and 0.94, the systolic linear model created is seen by equation 21 and the diastolic linear model created is seen by equation 22. The systolic model gave a MSE of 8.457e-09 and R^2 value of .9089. They diastolic model gave a MSE of 3.0350e-08 and R^2 value of 0.8602. These results show that the linear models created had very little error and strong correlation of the data.

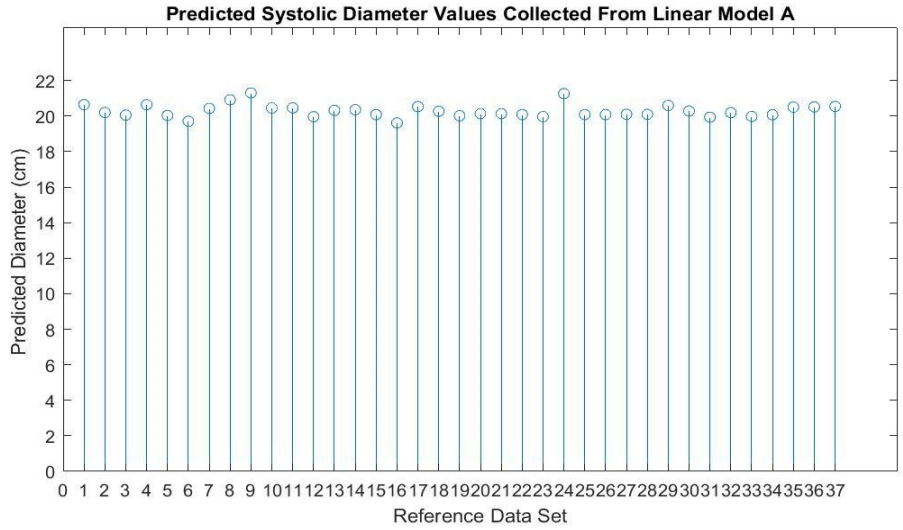

Figure 11: Stem plot of reference systolic diameter predictions based on linear model A

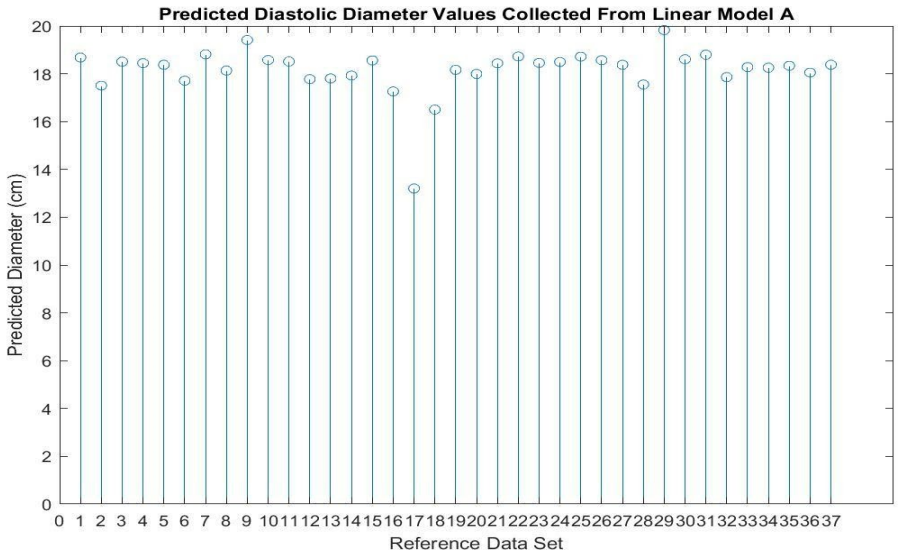

Figure 12: Stem plot of reference diastolic diameter predictions based on linear model A

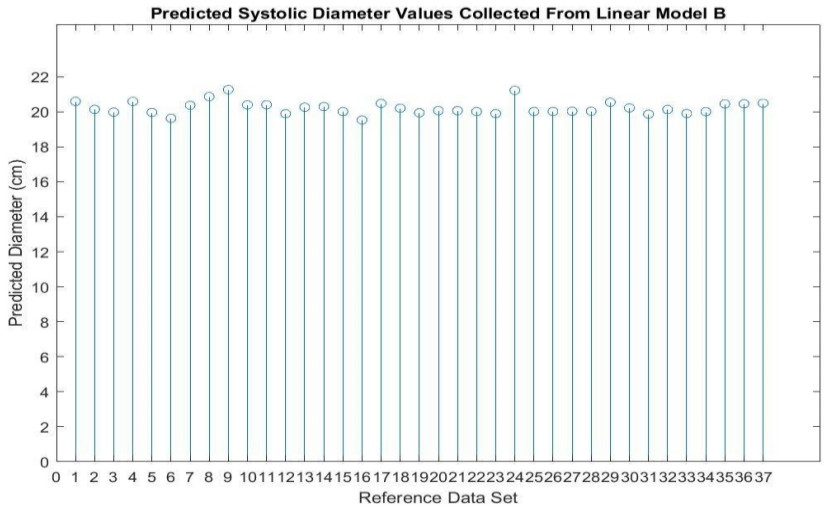

Figure 13: Stem plot of reference systolic diameter predictions based on linear model B

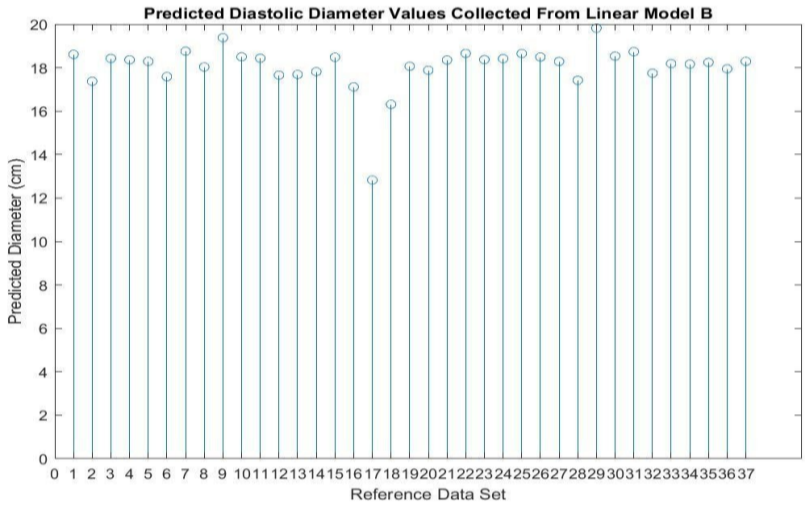

Figure 14: Stem plot of reference diastolic diameter predictions based on linear model B

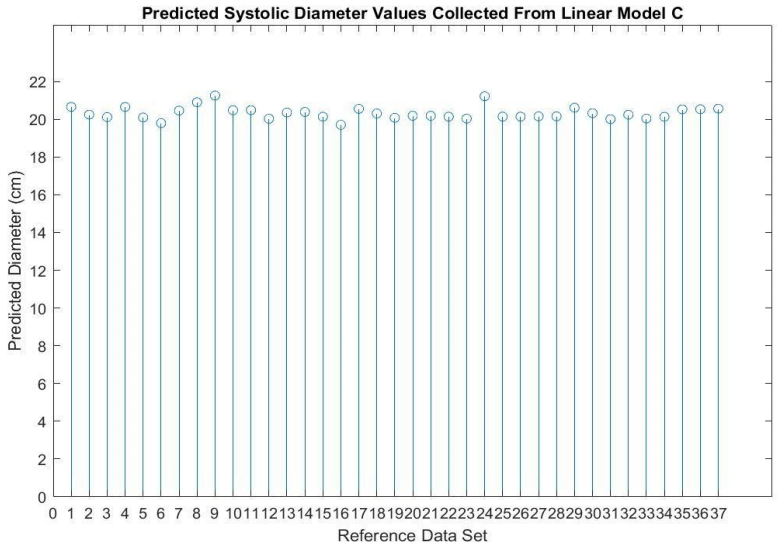

Figure 15: Stem plot of reference systolic diameter predictions based on linear model C

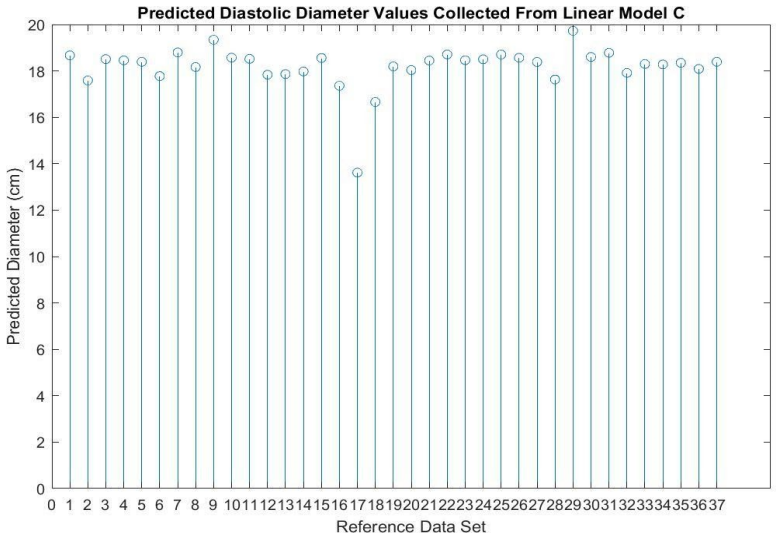

Figure 16: Stem plot of reference diastolic diameter predictions based on linear model C

As seen by Figures Figure 11, Figure 13, and Figure 15 all the systolic diameter predictions for the linear models fall between 19 to 21 cm, which is seen in the validation data for healthy adult aortic diameter ranges. However, for Figures Figure 12, Figure 14, and Figure 16 all the diastolic diameter predictions have a larger range as well as a very clear outlier for data set 17. The diastolic values range from 16 to 20 cm, except for the one outlier in each model. The outlier is between 12 to 13 cm, which is clinically abnormal for an adult human aorta. This outlier may be that the data came from a younger subject who has a smaller heart than the other subjects or the prediction may not work well for that waveform observed.

To get a better understanding of how the neural network model predictions compared to the validation study scatter plots of the neural network predicted diameters versus the validation diameters were plotted to see the correlation.

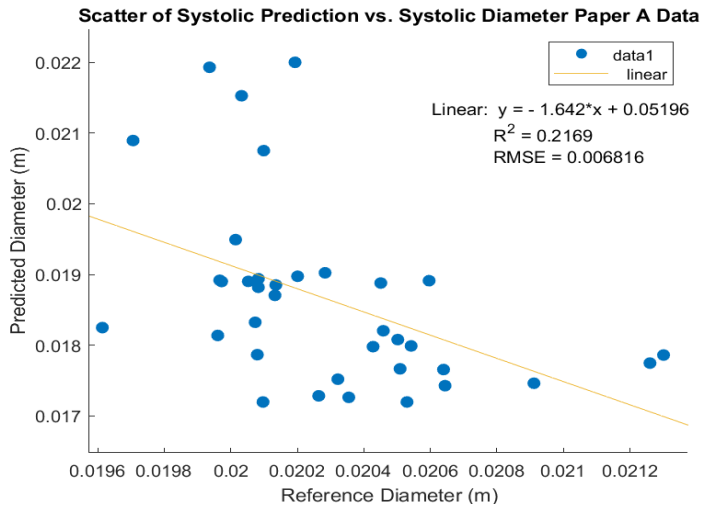

Figure 17: Scatter plot of the systolic diameter predictions from the proposed neural network versus the reference diameter from graph A

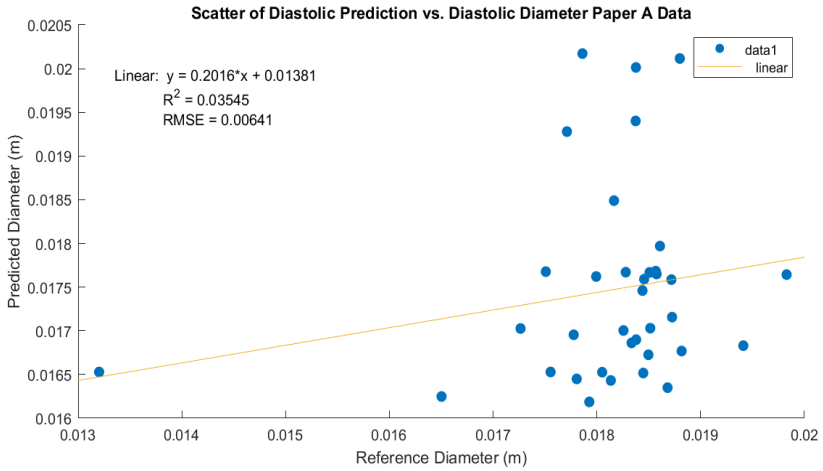

Figure 18: Scatter plot of the diastolic diameter predictions from the proposed neural network versus the reference diameter from graph A

For Model A, the systolic correlation against the predicted diameters was 0.2169 and the diastolic correlation against the predicted diameters was 0.03545 as seen by Figure 17 and Figure 18, respectively. These results show that there is low to moderate correlation between the systolic diameters predicted by the neural network compared to the validated reference diameters from the Stefanadis *et. al* study but there is very poor correlation between the diastolic diameter predictions. This shows that the neural network is a poor predictor of diastolic aortic diameter but could potentially be used for systolic aortic diameter predictions once further testing is conducted.

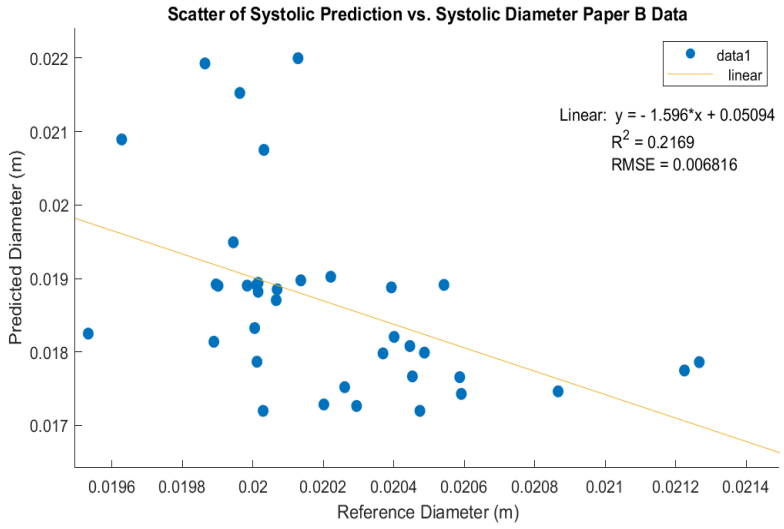

Figure 19: Scatter plot of the systolic diameter predictions from the proposed neural network versus the reference diameter from graph B

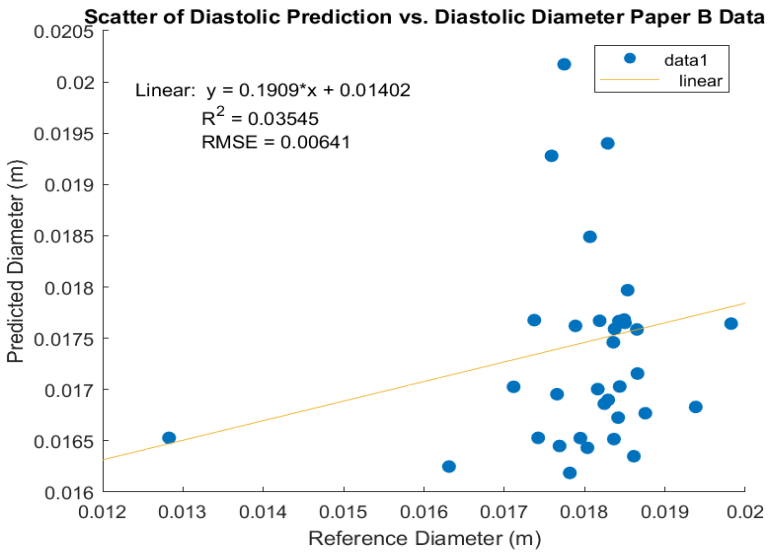

Figure 20: Scatter plot of the diastolic diameter predictions from the proposed neural network versus the reference diameter from graph B

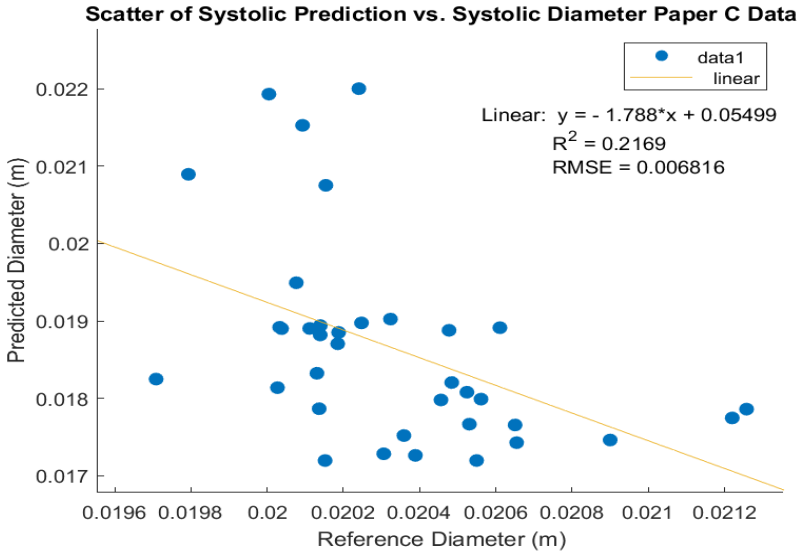

Figure 21: Scatter plot of the systolic diameter predictions from the proposed neural network versus the reference diameter from graph C

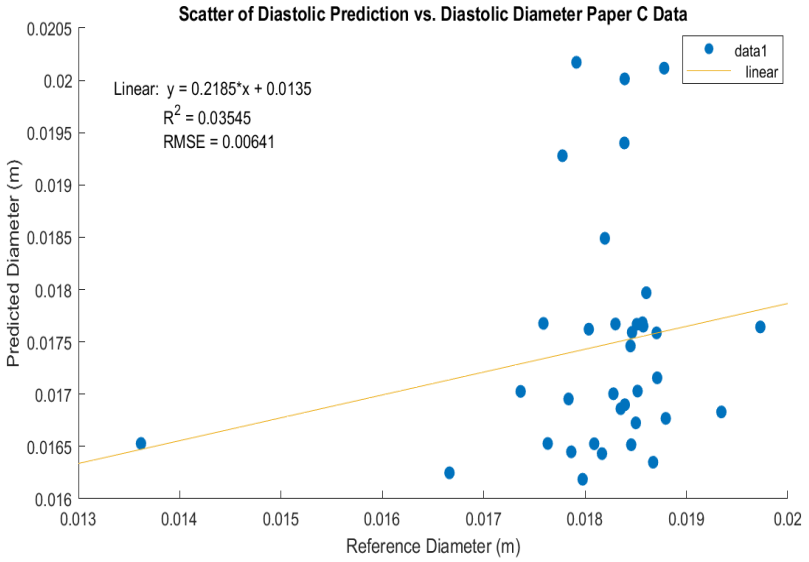

Figure 22: Scatter plot of the diastolic diameter predictions from the proposed neural network versus the reference diameter from graph B

For Model B and C, the systolic correlation against the predicted diameters were also 0.2169 and the diastolic correlation against the predicted diameters were 0.03545, which was the same as seen in Model A as seen by Figure 19, Figure 20,Figure 21, and Figure 22. These results also show that there is moderate correlation between the systolic diameters predicted by the neural network compared to the validated reference diameters from the Stefanadis *et. al* study but there is very poor correlation between the diastolic diameter predictions. These exact same values for correlation can be explained by the fact that the graphs referenced have very little difference between the values observed and the validation study was only conducted on one human subject, thus one would not expect there to be any change in the diameters observed in one subject in small time variances of 30 minutes.

Next, the spearman correlation function was performed on the 6 linear models (A, B, C) that have a systolic and diastolic model as discussed above. The spearman correlations were found to be the same for all the systolic models as well as the same for all the diastolic models as well. The MATLAB function "corr" was utilized to give the correlation between the reference predictions from the linear models and the neural network predicted diameters. For the systolic models, the spearman correlation was -0.5664 and the diastolic models had a spearman correlation of 0.1932. This shows that the neural network and reference data have a moderate negative correlation for systolic predictions but a low positive correlation for the diastolic predictions. These results help solidify the results from before that the neural network may be able to predict systolic aorta diameter after more validation studies are performed on a larger database.

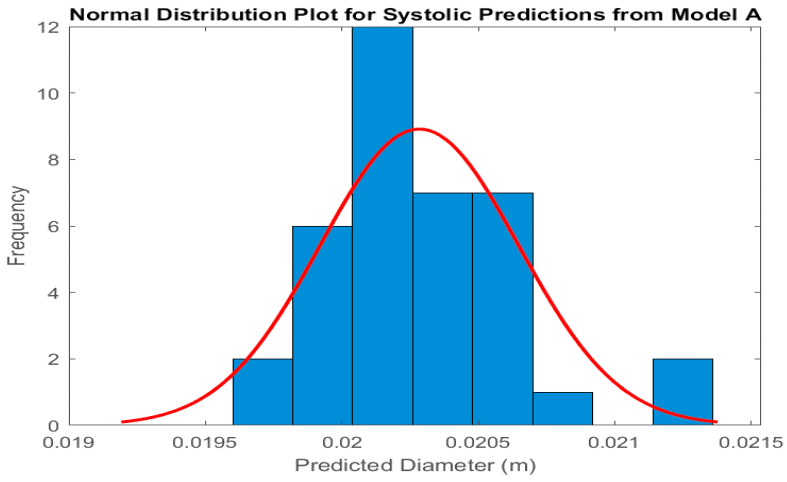

Figure 23: Normal distribution plot of the systolic diameter predictions from the proposed neural network from graph A

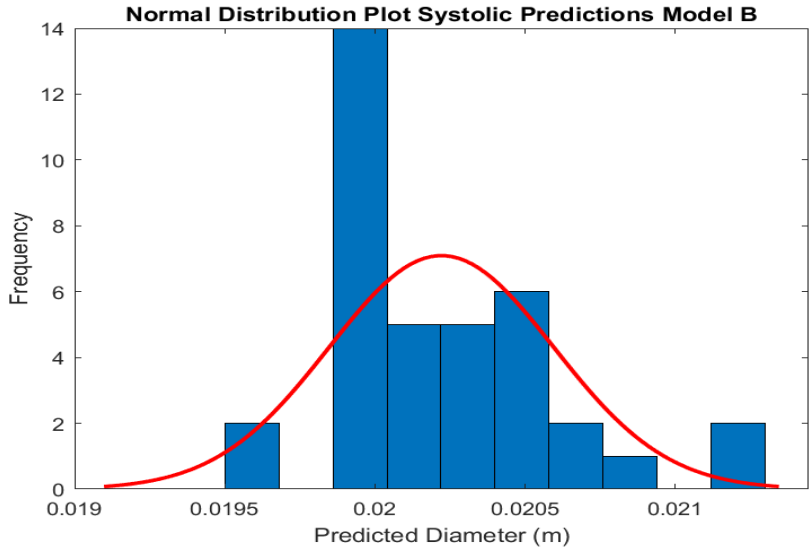

Figure 24: Normal distribution plot of the systolic diameter predictions from the proposed neural network from graph B

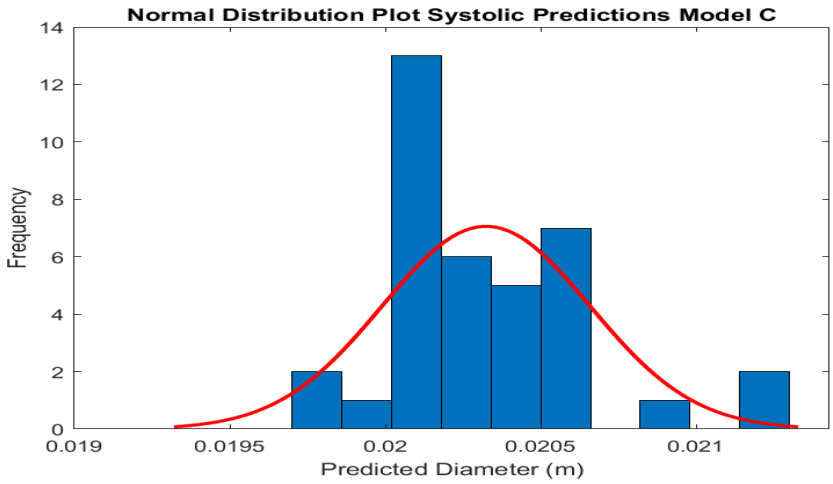

Figure 25: Normal distribution plot of the systolic diameter predictions from the proposed neural network from graph C

Figure 23, Figure 24, and Figure 25 show that the distributions for the systolic diameter predictions are skewed right. This means that the distribution ranges are not

normal, thus the Kruskal-Wallis ANOVA test is the appropriate test to perform on the systolic predicted data.

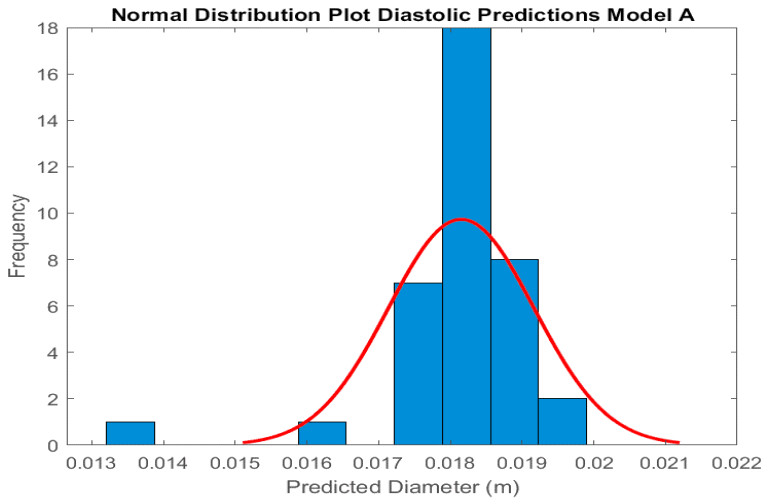

Figure 26: Normal distribution plot of the diastolic diameter predictions from the proposed neural network from graph A

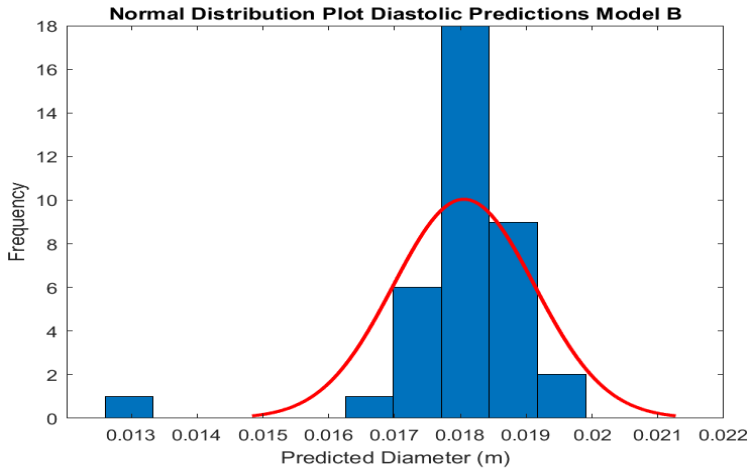

Figure 27: Normal distribution plot of the diastolic diameter predictions from the proposed neural network from graph B

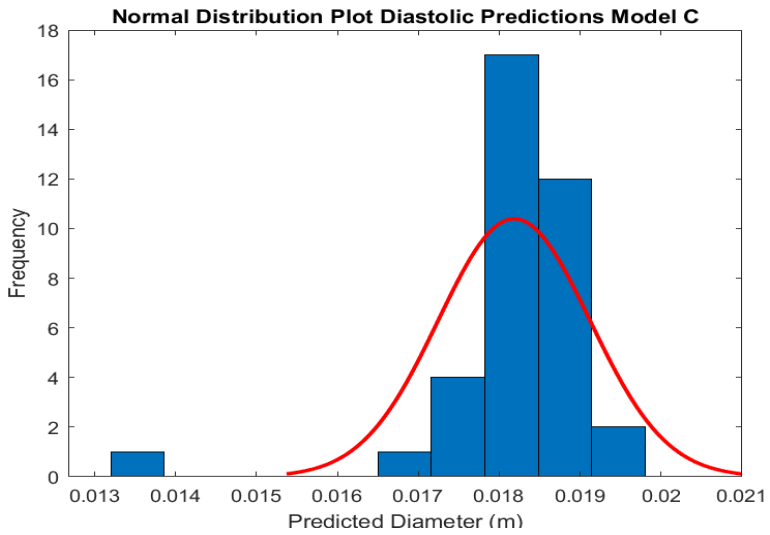

Figure 28: Normal distribution plot of the diastolic diameter predictions from the proposed neural network from graph C

Figure 26, Figure 27, and Figure 28 show that the distributions for the diastolic diameter predictions are skewed left. This also means that the distribution ranges are not normal, thus the Kruskal-Wallis ANOVA test is the appropriate test to perform on the diastolic predicted data as well.

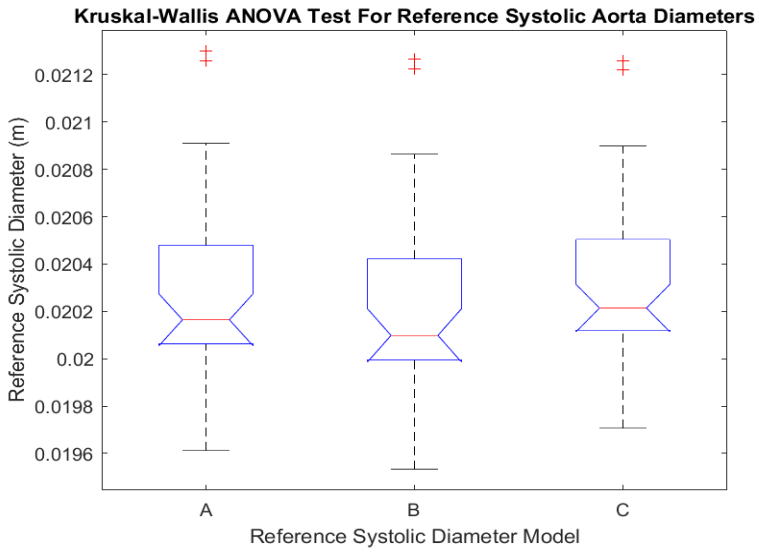

Figure 29: Graph of Kruskal-Wallis ANOVA test for reference systolic aorta diameters

Kruskal-Wallis ANOVA Table

Source	SS	df	MS	Chi-sq	Prob>Chi-sq
Columns	3873.1	2	1936.54	3.74	0.1542
Error	110086.9	108	1019.32		
Total	113960	110			

Figure 30: Kruskal-Wallis ANOVA test for reference systolic aorta diameters table data

Figure 29 shows that there are 2 finite outliers observed from the reference systolic diameter models. Figure 30 shows that the p value for the systolic models is 0.1542. This means that the null hypothesis is not rejected at a 10% significance level, meaning that there is strong evidence to show that the results are not random and there is not a statistically significant difference. This means that the data comes from different populations with the same distribution of aorta systolic diameters.

Since the p value is larger than the significance level tested at these outliers would not impact the conclusions drawn for this data.

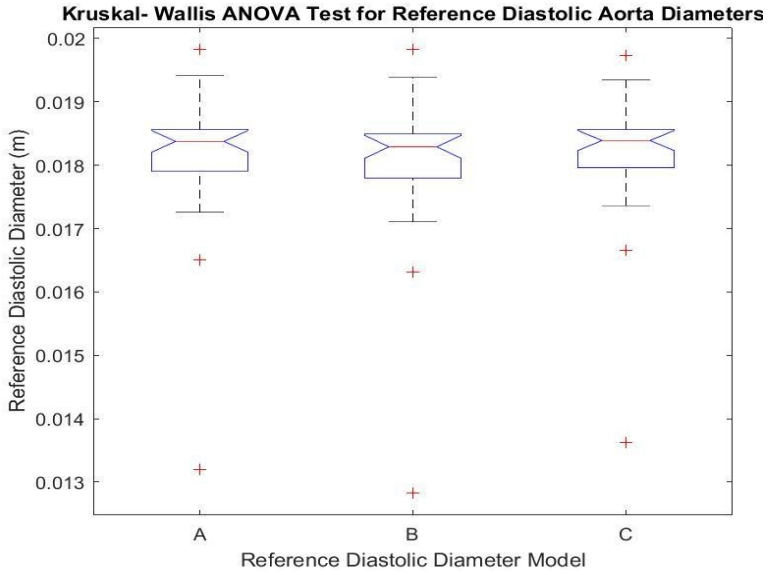

Figure 31: Graph of Kruskal-Wallis ANOVA test for reference diastolic aorta diameters

Kruskal-Wallis ANOVA Table

Source	SS	df	MS	Chi-sq	Prob>Chi-sq
Columns	1253.6	2	626.78	1.21	0.5461
Error	112706.4	108	1043.58		
Total	113960	110			

Figure 32: Kruskal-Wallis ANOVA test for reference diastolic aorta diameters table data

Figure 31 shows that there are 3 finite outliers observed from the reference diastolic diameter models as well. This makes sense as 2 outliers were observed from the systolic models as well and it was already observed that there was a major outlier

seen between 12 and 13 cm so it makes sense that there would be an extra outlier with the diastolic diameters. Figure 32 shows that the p value for the systolic models is 0.5461. This means that the null hypothesis is not rejected at a 10% significance level, meaning that there is strong evidence to show that the results are not random and come from different populations with the same distribution of aorta diastolic diameters. Since the p value is larger than the significance level tested at these outliers would not impact the conclusions drawn for this data.

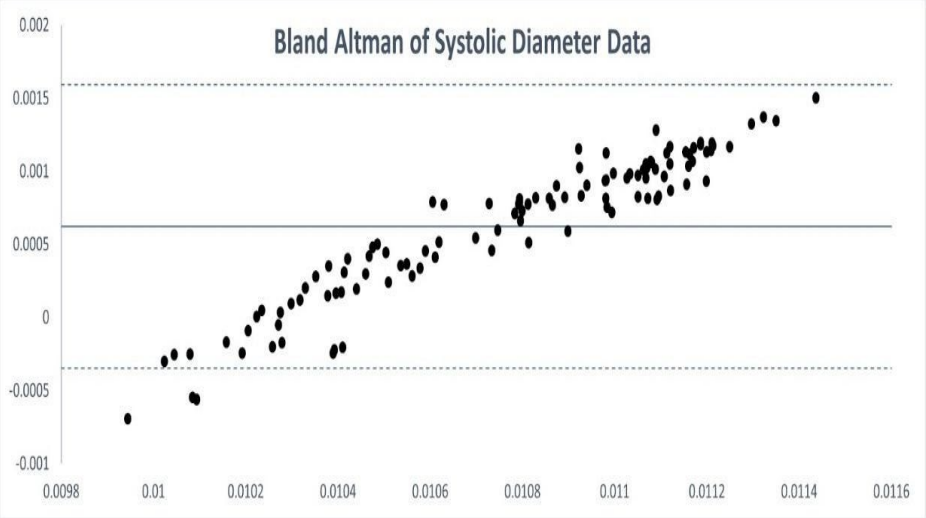

Figure 33: Bland Altman analysis of the predicted systolic diameter data

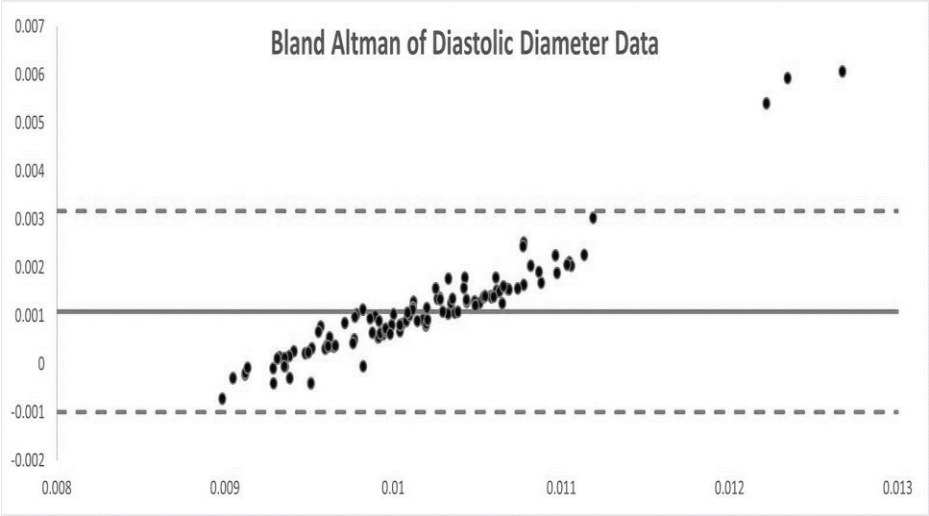

Figure 34: Bland Altman analysis of the predicted diastolic diameter data

These Bland Altman graphs show that only 3 data points fall outside of the 95% limits of agreement in both the systolic or diastolic plots as seen by Figure 33 and Figure 34 respectively. Both figures show a large linear spread, which allows one to conclude that there is no clear bias seen in the data. These graphs also show that there is strong agreement in both plots as 97.3% of the data are contained in the limits of agreement. This allows one to conclude that there is a both a clear relationship as well as no bias between the predicted and reference diameter data collected for both systolic and diastolic diameter data.

3.3 First Validation Study Trial 2 Results

Using the same figure 5 in the Stefanadis *et. al* paper, the clear outlier in data set 17 was removed to determine if the correlations for the diastolic diameters would improve.

The linear models were again found using the MATLAB function “fitlm”.

$$\text{Systolic Model A: } y = 2.0201e\text{-}05x + 0.00017402 \quad (23)$$

$$\text{Diastolic Model A: } y = 5.1121e\text{-}05x + 0.014568 \quad (24)$$

For graph A at regression values of 0.94 and 0.95, the systolic linear model created is seen by equation 23 and the diastolic linear model created is seen by equation 24. The systolic model has a MSE of 1.0650e-08 and a R value of 0.8882. The diastolic model for graph A had an MSE of 2.2196e-08 and a R^2 value of 0.9052.

$$\text{Systolic Model B: } y = 2.0772e\text{-}05x + 0.01785 \quad (25)$$

$$\text{Diastolic Model B: } y = 5.3986e\text{-}05x + 0.014268 \quad (26)$$

For graph B at regression values of 0.94 and 0.93, the systolic linear model created is seen by equation 25 and the diastolic linear model created is seen by equation 26. the systolic model yielded a MSE of 1.2096e-08 and R^2 value 0.8909. The diastolic model for graph B yielded a MSE of 3.3795e-08 and R^2 value of .08722.

Systolic Model C: y = 1.8552e-05 + 0.018205 (27)

Diastolic Model C: y = 4.7161e-05x + 0.014877 (28)

For graph C, at regression values of 0.95 and 0.94, the systolic linear model created is seen by equation 27 and the diastolic linear model created is seen by equation 28. The systolic model gave a MSE of 8.4567e-09 and R^2 value of .9089. They diastolic model gave a MSE of 3.0350e-08 and R^2 value of 0.8602. These results show that the linear models created had very little error and strong correlation of the data.

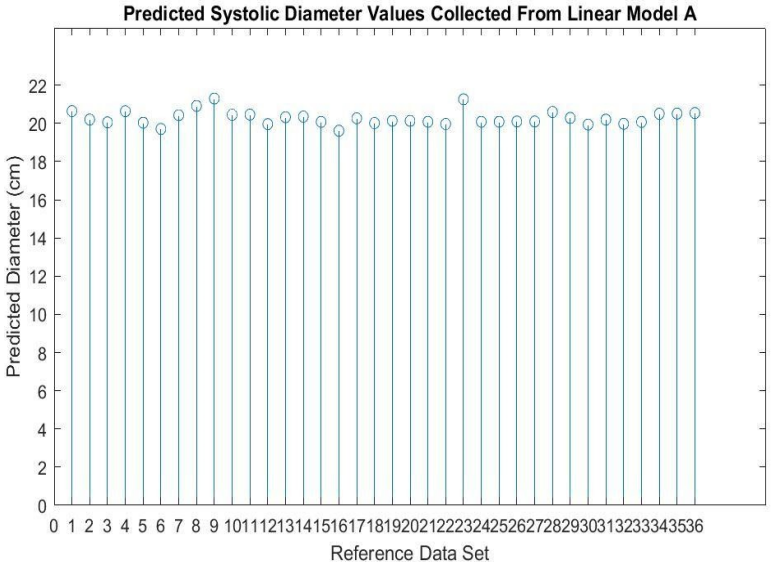

Figure 35: Stem plot of reference systolic diameter predictions based off the linear model A in the first validation study with the outlier removed

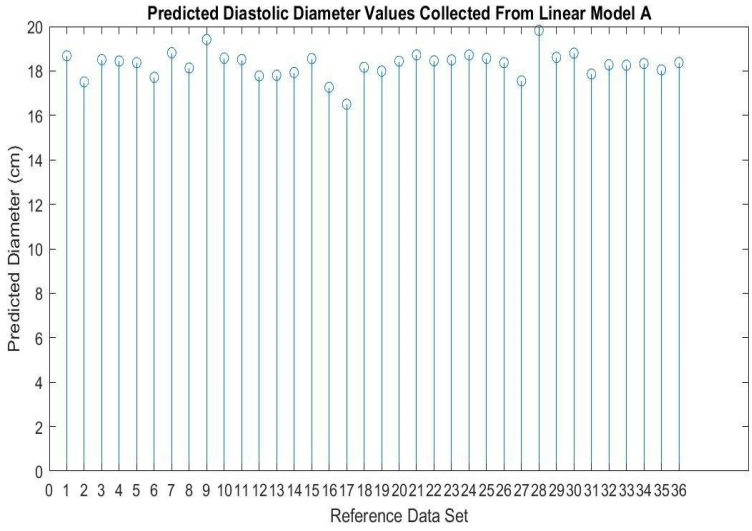

Figure 36: Stem plot of reference diastolic diameter predictions based off the linear model A in the first validation study with the outlier removed

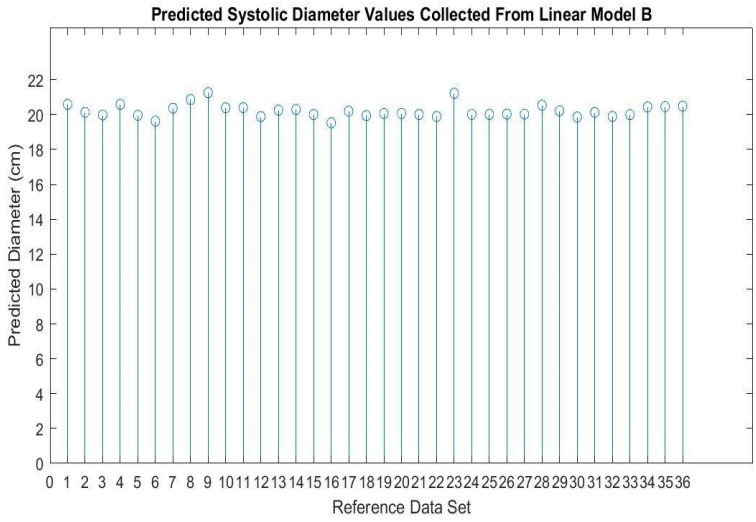

Figure 37: Stem plot of reference systolic diameter predictions based off the linear model B in the first validation study with the outlier removed

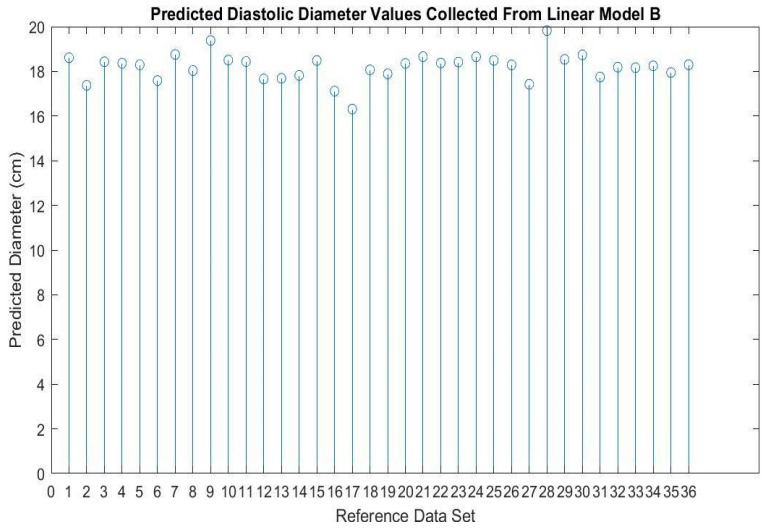

Figure 38: Stem plot of reference diastolic diameter predictions based off the linear model B in the first validation study with the outlier removed

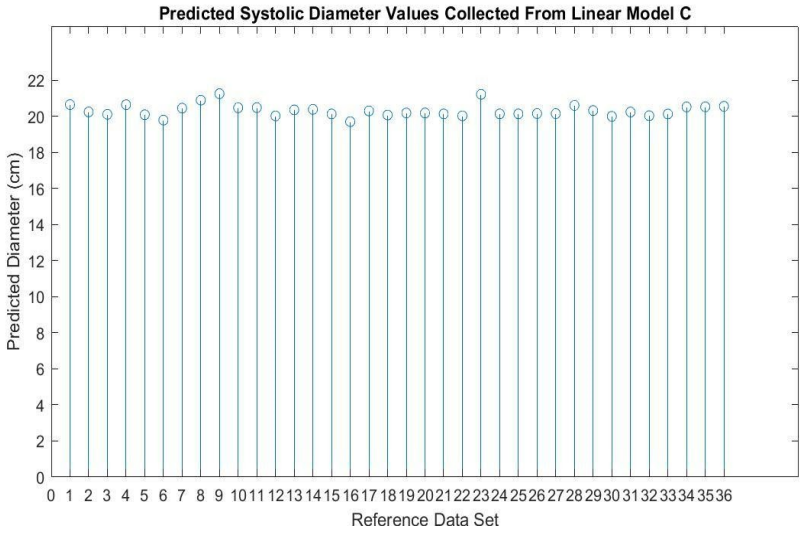

Figure 39: Stem plot of reference systolic diameter predictions based off the linear model C in the first validation study with the outlier removed

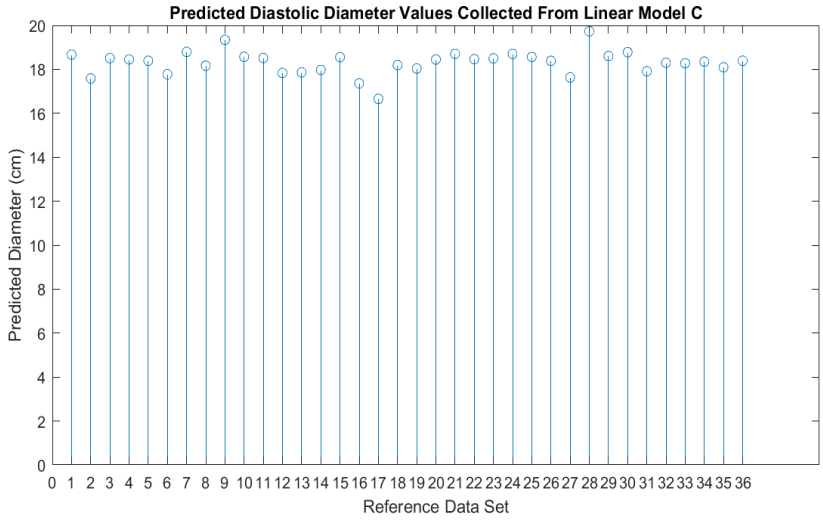

Figure 40: Stem plot of reference diastolic diameter predictions based off the linear model C in the first validation study with the outlier removed

As seen by Figure 35, Figure 37, and Figure 39 all the systolic diameter predictions for the linear models fall between 19 to 21 cm, which again is seen in the validation data for healthy adult aortic diameter ranges. Now for Figure 36, Figure 38, and Figure 40 all the diastolic diameter predictions have a larger range from 16 to 20 cm and there is no clear outlier being observed from the remaining 36 data sets.

Now with the outlier removed, scatter plots are utilized to get a better understanding of how the neural network model predicts compared to the validation study. The scatter plots are of the neural network predicted diameters versus the validation diameters were constructed to see the correlation between the systolic and diastolic values.

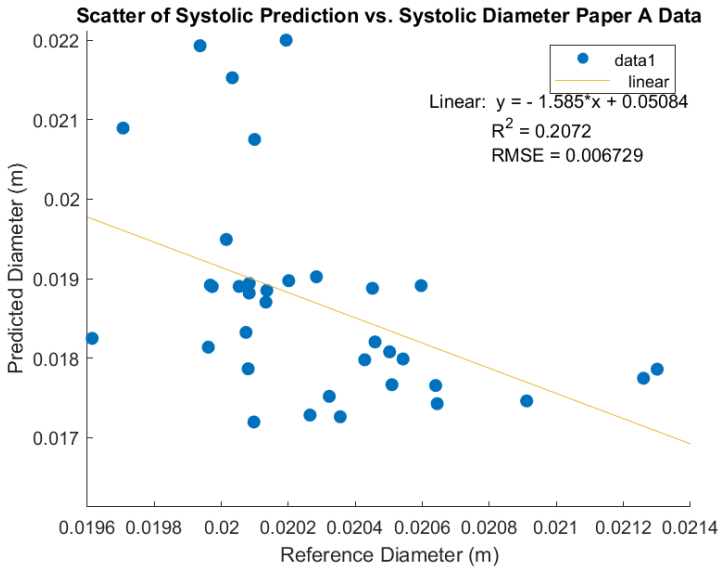

Figure 41: Scatter plot of the systolic diameter predictions from the proposed neural network versus the reference diameter from graph A with outlier removed

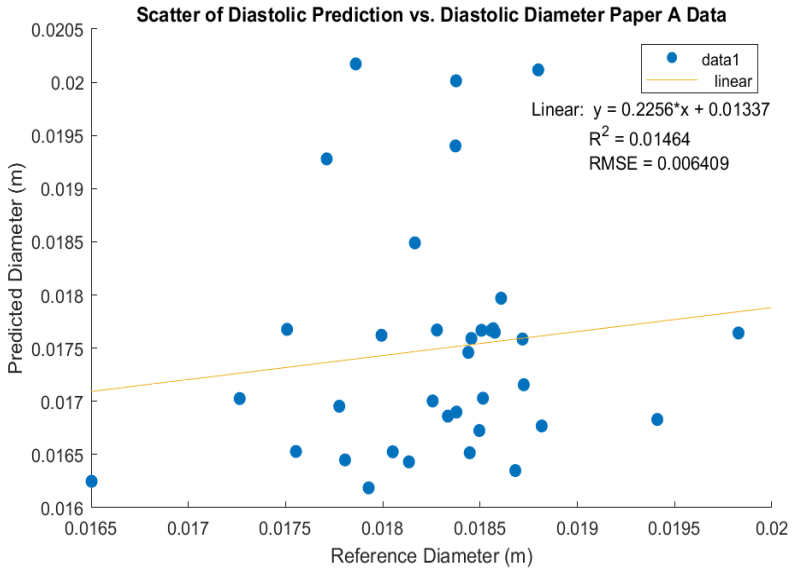

Figure 42: Scatter plot of the diastolic diameter predictions from the proposed neural network versus the reference diameter from graph A with outlier removed

For Model A, the systolic predicted diameters correlation was found to have a R^2 value of 0.2076, as seen by Figure 41, which was slightly lower than the previous run with the outlier as it yielded a R^2 value of 0.2169. The diastolic correlation against the predicted diameters was observed to have a R^2 value of .01464, as seen by Figure 42, which was much lower than previously observed with the outlier as it had a R^2 value 0.03545. These results show that there is low to moderate correlation between the systolic diameters predicted by the neural network compared to the validated reference diameters from the Stefanadis *et. al* study but there is very poor correlation between the diastolic diameter predictions. This shows that the neural network is a poor predictor of diastolic aortic diameter but could potentially be used for systolic aortic diameter predictions once further testing is conducted.

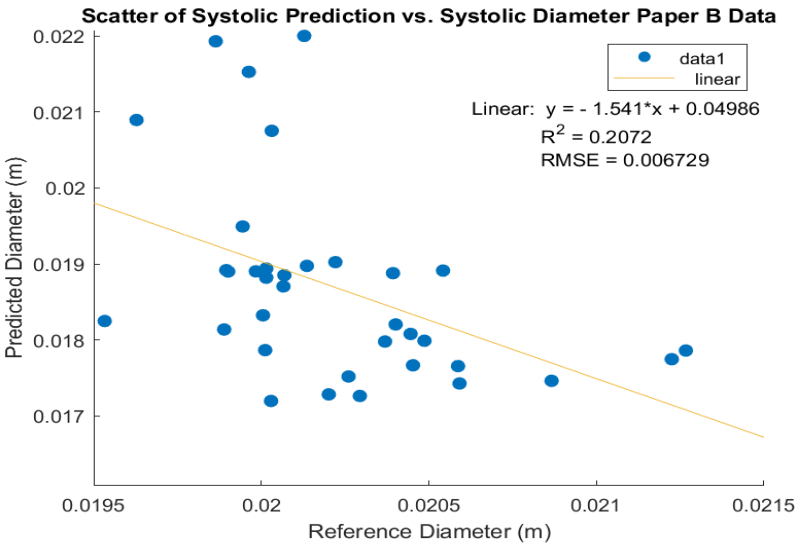

Figure 43: Scatter plot of the systolic diameter predictions from the proposed neural network versus the reference diameter from graph B with outlier removed

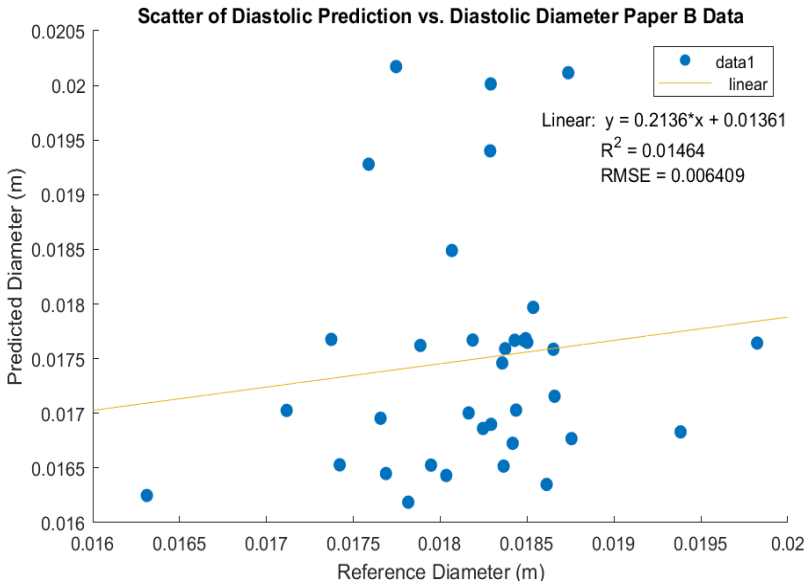

Figure 44: Scatter plot of the diastolic diameter predictions from the proposed neural network versus the reference diameter from graph B with outlier removed

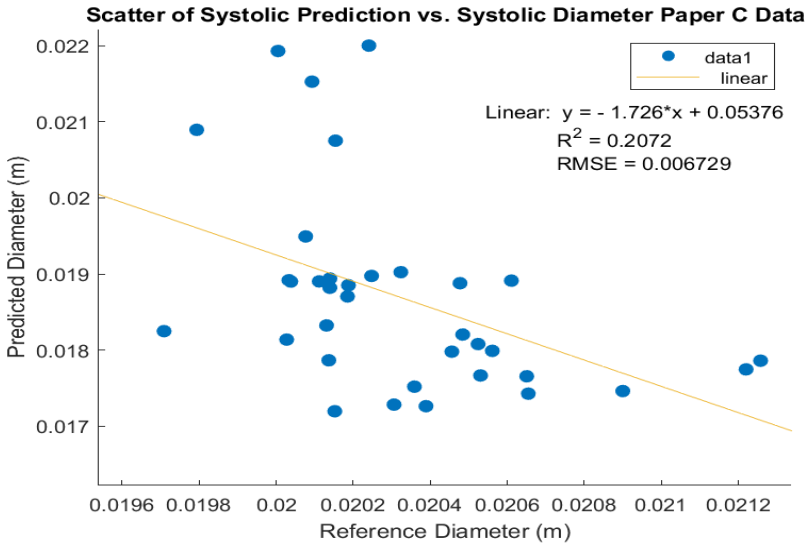

Figure 45: Scatter plot of the systolic diameter predictions from the proposed neural network versus the reference diameter from graph C with outlier removed

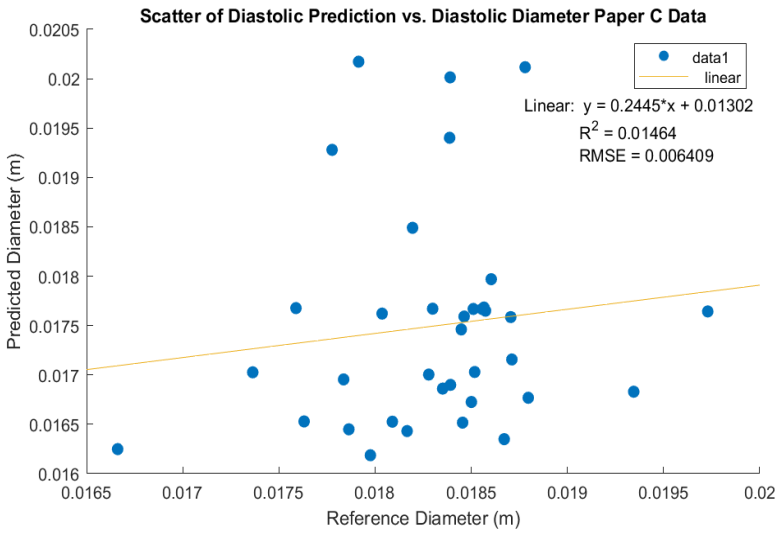

Figure 46: Scatter plot of the diastolic diameter predictions from the proposed neural network versus the reference diameter from graph C with outlier removed

For Model B and C, the systolic correlation against the predicted diameters were also 0.2076 and the diastolic correlation against the predicted diameters were 0.01464, which was the same as seen in Model A as seen by Figure 43, Figure 44, Figure 45 and Figure 46. These results also show that there is now less of a moderate correlation between the systolic diameters predicted by the neural network compared to the validated reference diameters from the Stefanadis *et. al* study and there is even lower poor correlation between the diastolic diameter predictions. These findings were surprising as the hope was that by removing the outlier, that the diastolic correlations would have been more positive. These exact same values for correlation can again be explained by the fact that the graphs referenced have very little difference between the values observed and the validation study was only conducted

on one human subject, thus one would not expect there to be any change in the diameters observed in one subject in small time variances of 30 minutes.

Next, the spearman correlation function was performed on the 6 linear models (A, B, C) as each model has a systolic and diastolic model. The spearman correlations were found to be the same for all the systolic models as well as the same for all the diastolic models as well. The MATLAB function "corr" was utilized to give the correlation between the reference predictions from the linear models and the neural network predicted diameters. For the systolic models, the spearman correlation was -0.5483, which was again slightly lower than previously observed with the outlier included as its spearman correlation was -0.5664. The diastolic models had a spearman correlation of 0.1475 which again was lower than previously observed as its spearman correlation was 0.1932. This shows that the neural network and reference data have a lower moderate negative correlation for systolic predictions but an even lower positive correlation for the diastolic predictions. These lower than anticipated results show the need to perform further testing of the neural network to determine if it may be able to predict systolic aorta diameter after more validation studies are performed on a larger database.

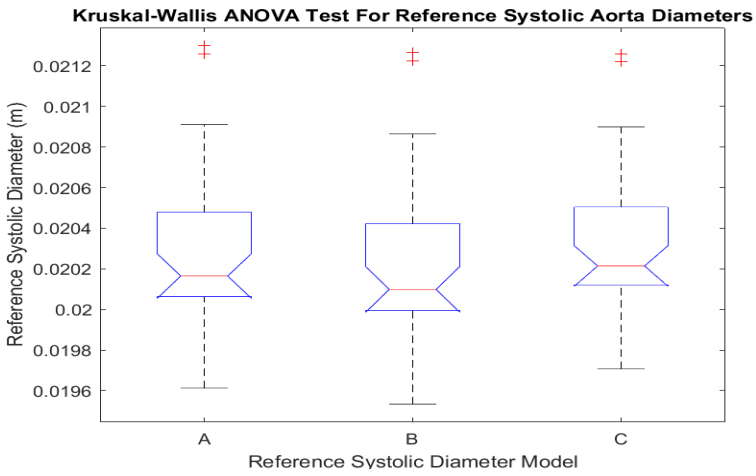

Figure 47: Graph of Kruskal-Wallis ANOVA test for reference systolic aorta diameters with outlier removed

Kruskal-Wallis ANOVA Table

Source	SS	df	MS	Chi-sq	Prob>Chi-sq
Columns	3702.1	2	1851.03	3.77	0.1515
Error	101264.9	105	964.43		
Total	104967	107			

Figure 48: Kruskal-Wallis ANOVA test for reference systolic aorta diameters table data with outlier removed

Figure 47 shows that there are 2 finite outliers observed from the reference systolic diameter models. Figure 48 shows that the p value for the systolic models is 0.1515. This means that the null hypothesis is not rejected at a 10% significance level, meaning that there is strong evidence to show that the results are not random and there is not a statistically significant difference. This means that the data comes from different populations with the same distribution of aorta systolic diameters. To compare these results to the previous results that included the outlier, the p value was

0.1542 which is slightly higher but does not change the conclusion that these results come from different populations with the same distribution of aorta systolic diameters. Since the p value is larger than the significance level tested at these outliers would not impact the conclusions drawn for this data.

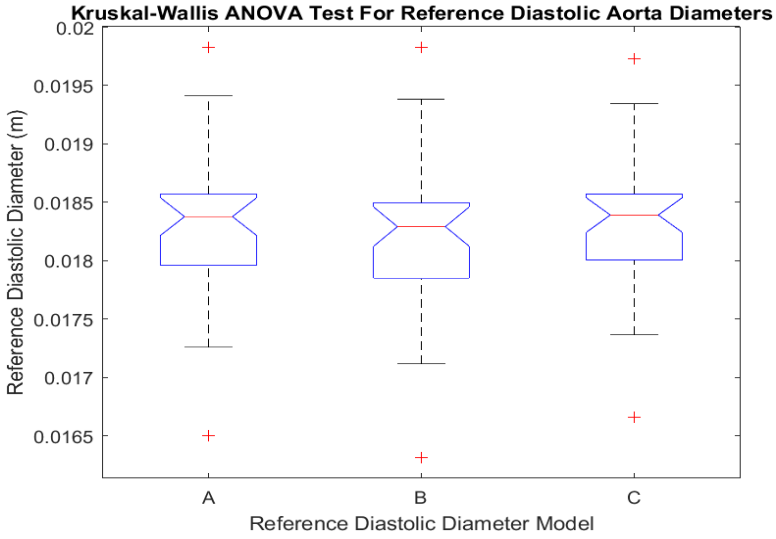

Figure 49: Graph of Kruskal-Wallis ANOVA test for reference diastolic aorta diameters with outlier removed

Kruskal-Wallis ANOVA Table

Source	SS	df	MS	Chi-sq	Prob>Chi-sq
Columns	1272.7	2	636.361	1.3	0.5227
Error	103694.3	105	987.565		
Total	104967	107			

Figure 50: Kruskal-Wallis ANOVA test for reference systolic aorta diameters table data with outlier removed

Figure 49 shows that there are 2 finite outliers observed from the reference diastolic diameter models as well now that the outlier was removed. Figure 50 shows

that the p value for the systolic models is 0.5227. This means that the null hypothesis is not rejected at a 10% significance level, meaning that there is strong evidence to show that the results are not random and come from different populations with the same distribution of aorta diastolic diameters. To compare these results to the previous results that included the outlier, the p value was 0.5461 which is again slightly higher but does not change the conclusion that these results come from different populations with the same distribution of aorta diastolic diameters as well. Since the p value is larger than the significance level tested at these outliers would not impact the conclusions drawn for this data.

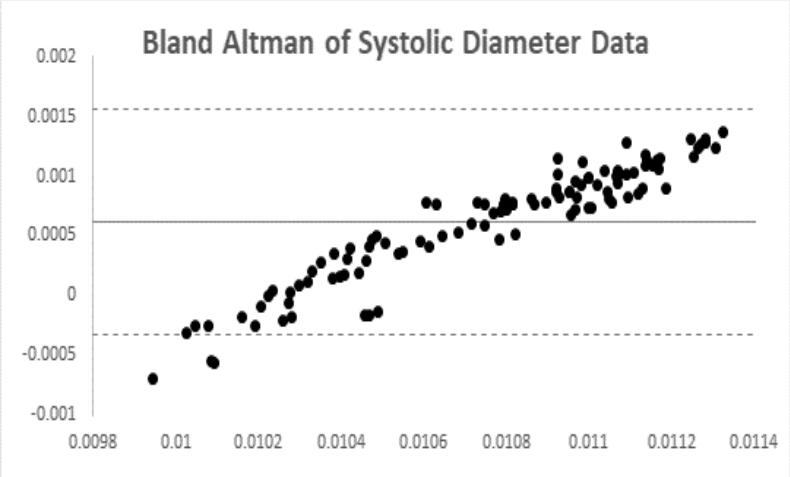

Figure 51: Bland Altman analysis of the predicted systolic diameter data with outlier removed

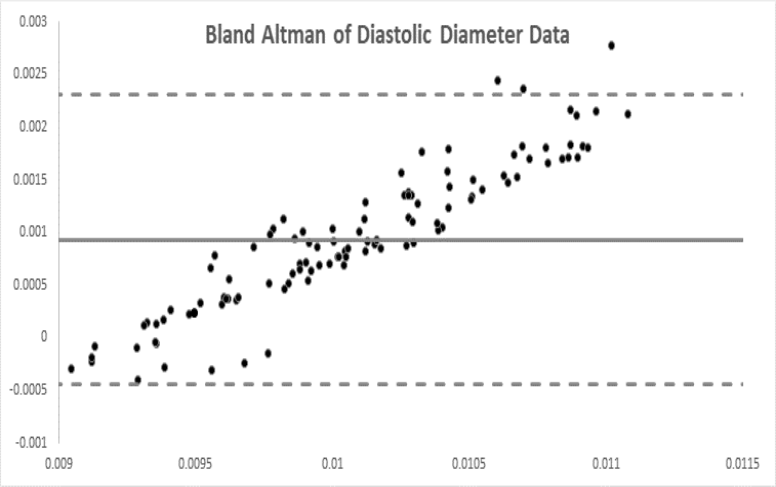

Figure 52: Bland Altman analysis of the predicted diastolic diameter data with outlier removed

These Bland Altman graphs again show that only 3 data points fall outside of the 95% limits of agreement in both the systolic or diastolic plots as seen by Figure 33 and Figure 34 as well as Figure 51 and Figure 52, respectively for Stefanadis *et. al* study. Both figures show a large linear spread, which allows one to conclude that there is no clear bias seen in the data. These graphs also show that there is strong agreement in both plots as 97.3% of the data are contained in the limits of agreement. This allows one to conclude that there certainly is both a clear relationship as well as no bias between the predicted and reference diameter data collected for both systolic and diastolic diameter data.

3.4 Second Validation Study Results

The following results will be based on the findings of the research article, by Länne *et al*., "Diameter and Compliance in the Male Human Abdominal Aorta: Influence of Age and Aortic Aneurysm". As observed during validation testing with study 1, the outlier dataset 17 was not used for this validation testing either.

Predicted Diameter Linear Models were created by using figure 4 in the Länne *et. al* paper using the WebPlotDigitizer to extract arterial pressure and aortic diameter measurements for 3 mean age groups: A- 25 years, B- 51 years, C- 70 years. One thing to note is that the figure does not allow for diastolic and systolic diameters to be seen but rather the mean aortic diameter only. Thus, there will only be 3 linear models of general mean diameter seen and not systolic and diastolic diameter.

The linear models were again found using the MATLAB function "fitlm".

$$\text{Diameter model A: } y = 2.016e\text{-}05x + 0.014935 \tag{29}$$

For graph A, mean 25 years, the average diameter linear model created is seen by equation 29. The diameter model has a MSE of 4.3450e-08 and a R^2 value of 0.9430.

$$\text{Diameter Model B: } y = 1.066e\text{-}05x + 0.016902 \tag{30}$$

For graph B, mean 51 years, the average diameter linear model created is seen by equation 30. The diameter model has a MSE of 4.0087e-09 and a R^2 value of 0.9761.

$$\text{Diameter Model C: } y = 7.1246e\text{-}06x + 0.020309 \quad (31)$$

For graph C, mean 70 years, the average diameter linear model created is seen by equation 31. The diameter model has a MSE of 4.6900e-09 and a R^2 value of 0.9400. These results also show that there is both minimal error and strong correlation of the data.

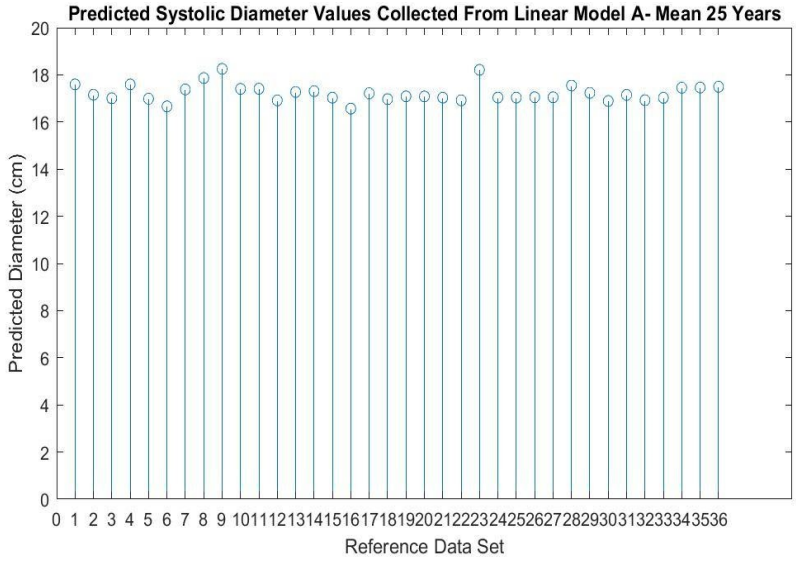

Figure 53: Stem plot of reference systolic diameter predictions based off the linear model A, mean 25 years, in the second validation study

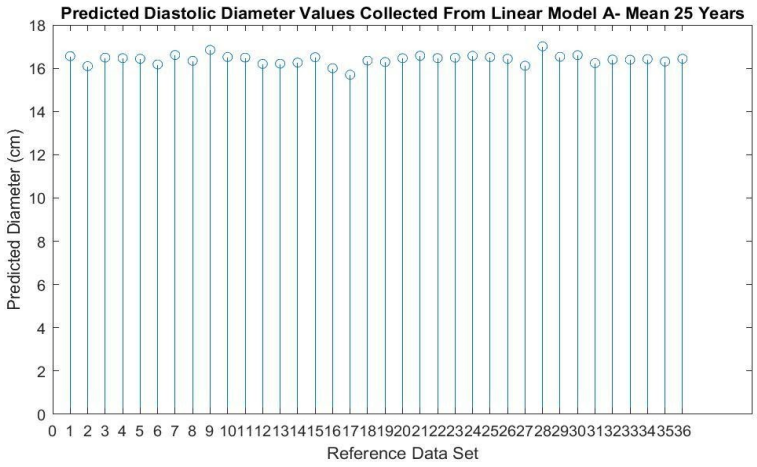

Figure 54: Stem plot of reference diastolic diameter predictions based off the linear model A, mean 25 years, in the second validation study

As seen by Figure 53, the reference systolic diameter predictions based on the mean age group of 25 years range from 16 to 18 cm. In Figure 54, the reference diastolic diameter predictions that are based on the mean age group of 25 years ranges from 16 to 17 cm.

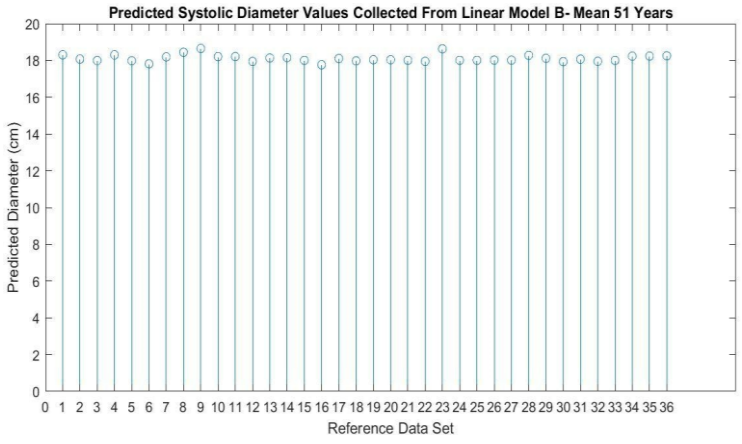

Figure 55: Stem plot of reference systolic diameter predictions based off the linear model B, mean 51 years, in the second validation study

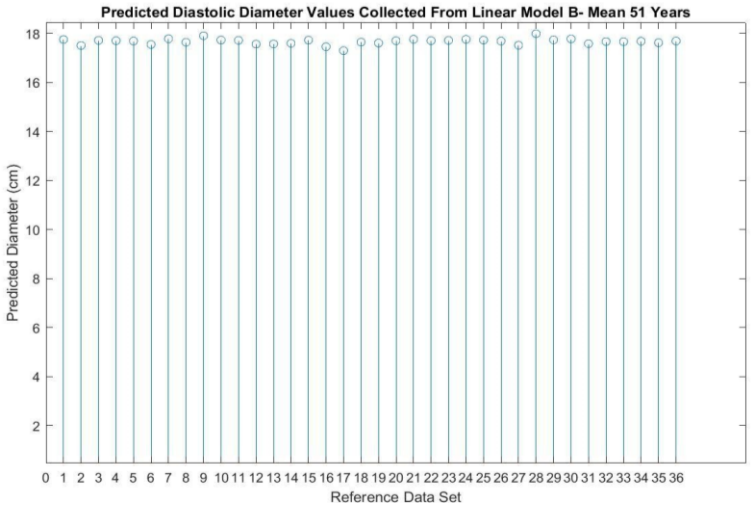

Figure 56: Stem plot of reference diastolic diameter predictions based off the linear model B, mean 51 years, in the second validation study

As seen by Figure 55, the reference systolic diameter predictions based on the mean age group of 51 years range from 17 to 18 cm. In Figure 56, the reference diastolic diameter predictions that are based on the mean age group of 51 years ranges from 17 to 18 cm.

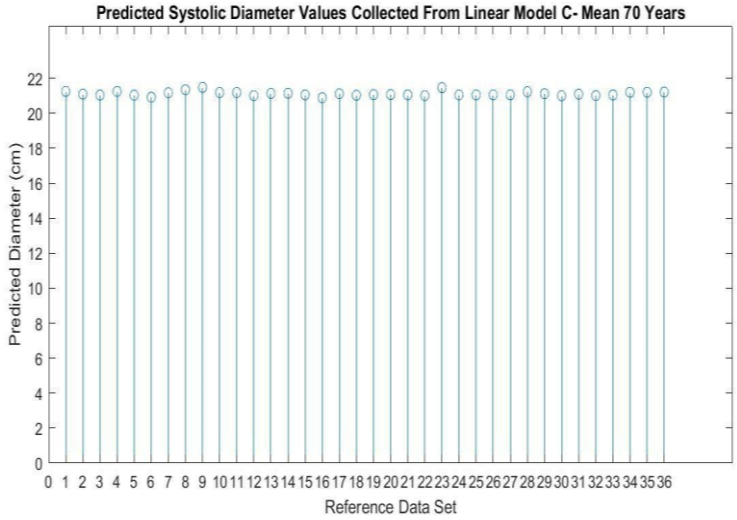

Figure 57: Stem plot of reference systolic diameter predictions based off the linear model C, mean 70 years, in the second validation study

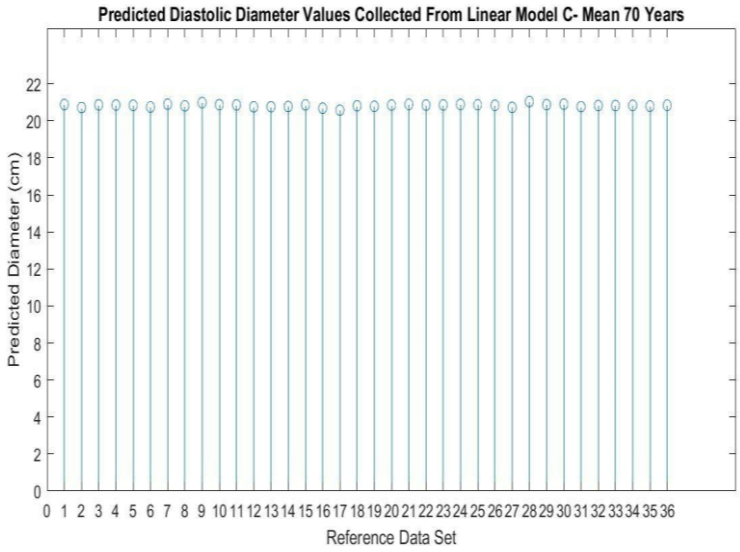

Figure 58: Stem plot of reference diastolic diameter predictions based off the linear model C, mean 70 years, in the second validation study

As seen by Figure 57, the reference systolic diameter predictions based on the mean age group of 70 years range from 20 to 21 cm. In Figure 58, the reference

diastolic diameter predictions that are based on the mean age group of 70 years ranges from 20 to 21 cm as well.

As seen by Figure 53, Figure 55, and Figure 57 the systolic diameter predictions for the linear models ranges increase as the mean age increases. This physiologically makes sense as humans age their aortic diameters will increase as the heart grows as the human grows. The same observation can be made regarding the diastolic diameter predictions for the linear models as seen by Figure 54, Figure 56, and Figure 58. It can also be noted that the diastolic diameters should be smaller in size than the systolic diameters, which is what is observed in all 3 linear model's data as well as in the validation testing performed using study 1.

Next, to get a better understanding of how the neural network model predictions compared to the validation study scatter plots of the neural network predicted diameters versus the validation diameters were plotted to see the correlation.

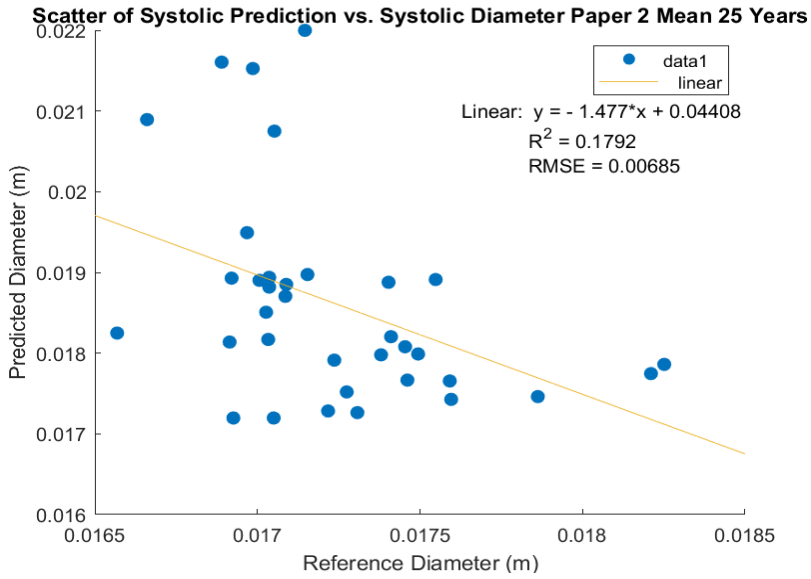

Figure 59: Scatter plot of the systolic diameter predictions from the proposed neural network versus the reference diameter from graph A for mean 25 years

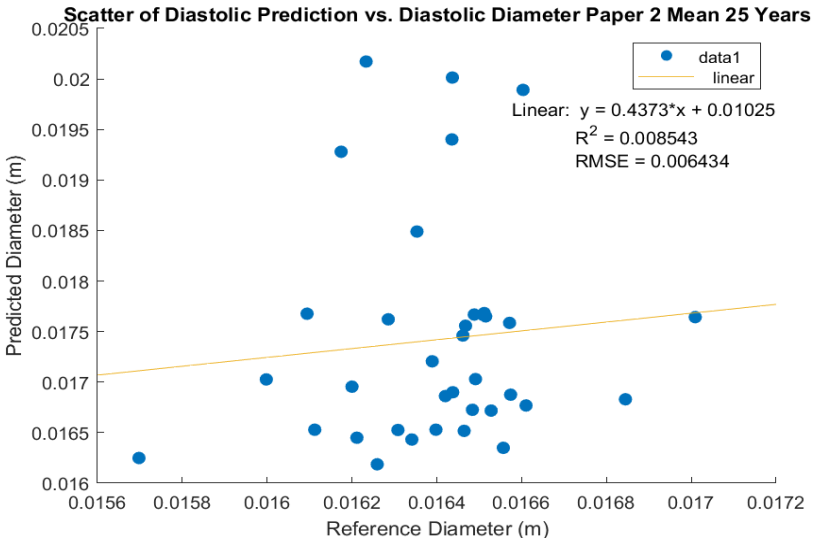

Figure 60: Scatter plot of the diastolic diameter predictions from the proposed neural network versus the reference diameter from graph A for mean 25 years

For Model A, the systolic correlation against the predicted diameters was 0.1792 and the diastolic correlation against the predicted diameters was 0.008543 as

seen by Figure 59 and Figure 60, respectively. These results show that there is low correlation between the systolic diameters predicted by the neural network compared to the validated reference diameters from the Stefanadis *et. al* study but there is practically no correlation between the diastolic diameter predictions. This shows that the neural network is again a poor predictor of diastolic aortic diameter but could potentially be used for systolic aortic diameter predictions once further testing is conducted, though the correlation is low.

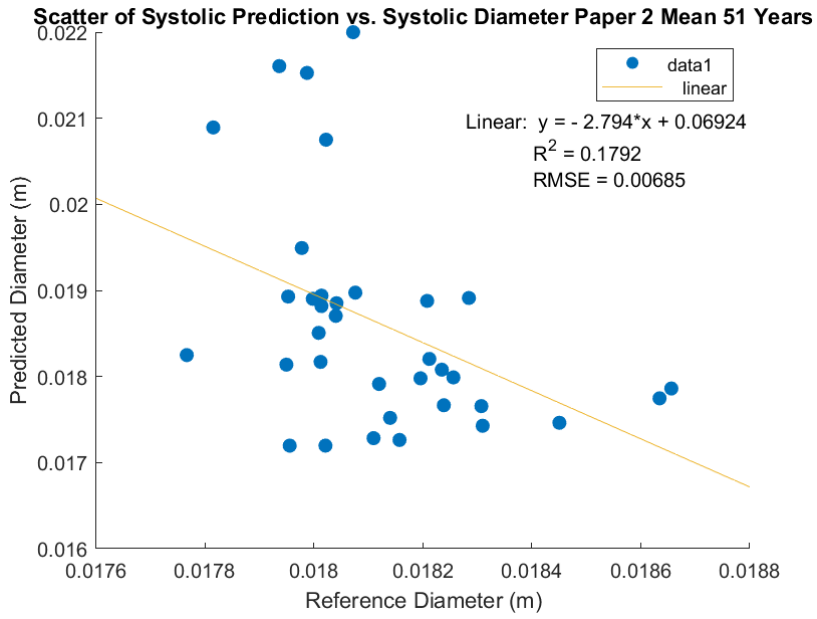

Figure 61: Scatter plot of the systolic diameter predictions from the proposed neural network versus the reference diameter from graph B for mean 51 years

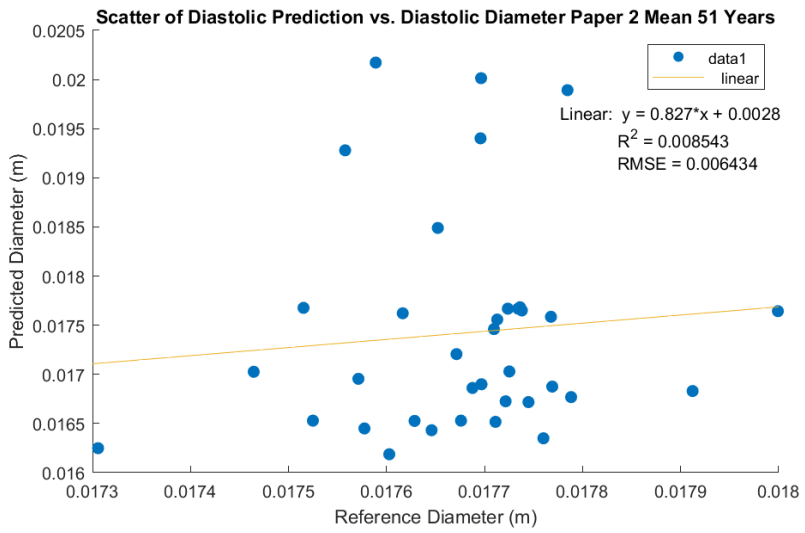

Figure 62: Scatter plot of the diastolic diameter predictions from the proposed neural network versus the reference diameter from graph B for mean 51 years

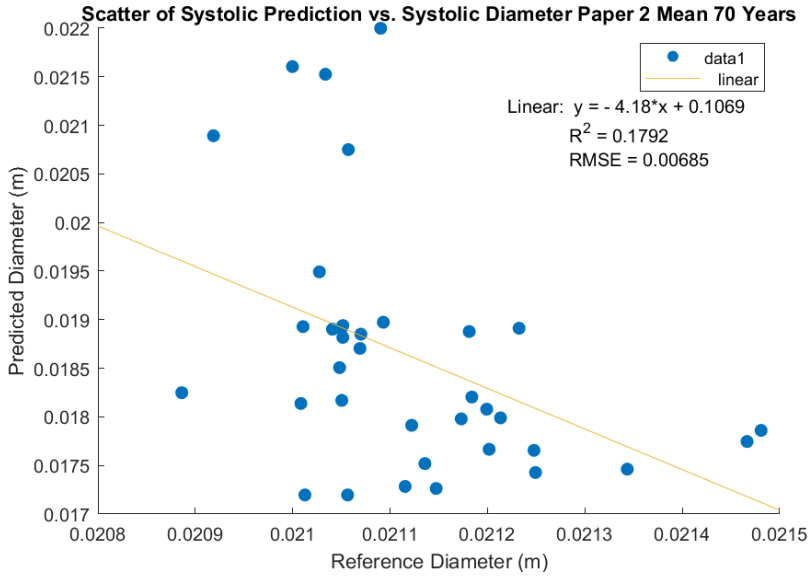

Figure 63: Scatter plot of the systolic diameter predictions from the proposed neural network versus the reference diameter from graph C for mean 70 years

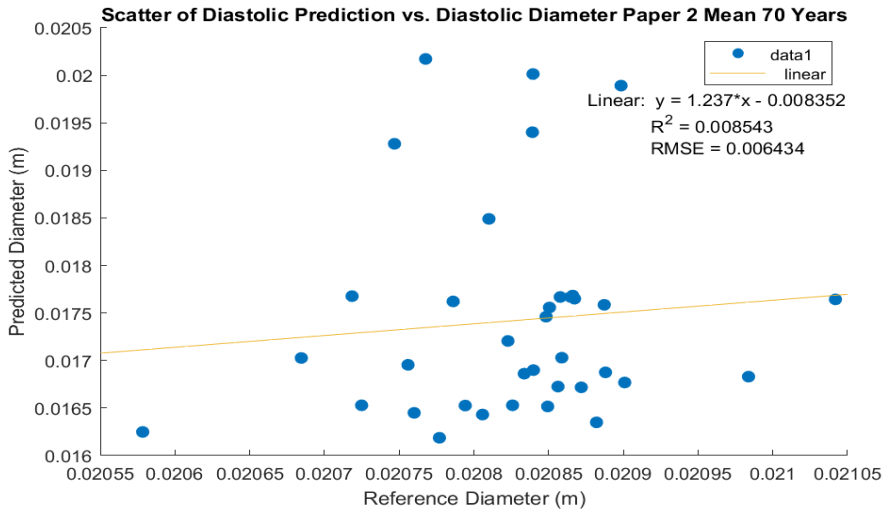

Figure 64: Scatter plot of the diastolic diameter predictions from the proposed neural network versus the reference diameter from graph C for mean 70 years

For Model B and C, the systolic correlation against the predicted diameters were also 0.1792 and the diastolic correlation against the predicted diameters were 0.008543, which was the same as seen in Model A as seen by Figure 61, Figure 62, Figure 63, and Figure 64. These results also show that there is low correlation between the systolic diameters predicted by the neural network compared to the validated reference diameters from the Länne *et. al* study but there is very poor to no correlation between the diastolic diameter predictions. These exact same values for correlation can be explained by the fact that the linear models were created using the same MATLAB function and reference database, so the predictions are very similar in range and have the same distribution of data just at higher diameter values as the mean age group increased.

Next, the spearman correlation function was performed on the 6 linear models (A, B, C) that have a systolic and diastolic model as discussed above. The spearman correlations were found to be the same for all the systolic models as well as the same for all the diastolic models as well. The MATLAB function "corr" was utilized to give the correlation between the reference predictions from the linear models and the neural network predicted diameters. For the systolic models, the spearman correlation was -0.4898 and the diastolic models had a spearman correlation of 0.1156 This shows that the neural network and reference data have a moderate negative correlation for systolic predictions but a low positive correlation for the diastolic predictions. These results again help solidify the results from study 1 that the neural network may be able to predict systolic aorta diameter after more validation studies are performed on a larger database.

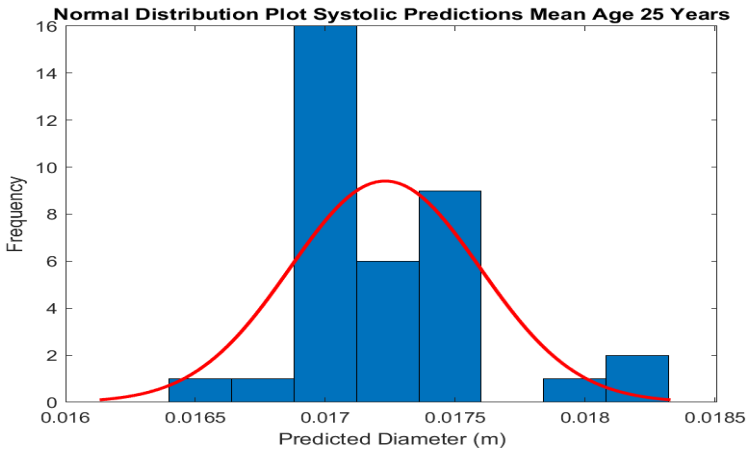

Figure 65: Normal distribution plot of the systolic diameter predictions from the proposed neural network from graph A for mean 25 years

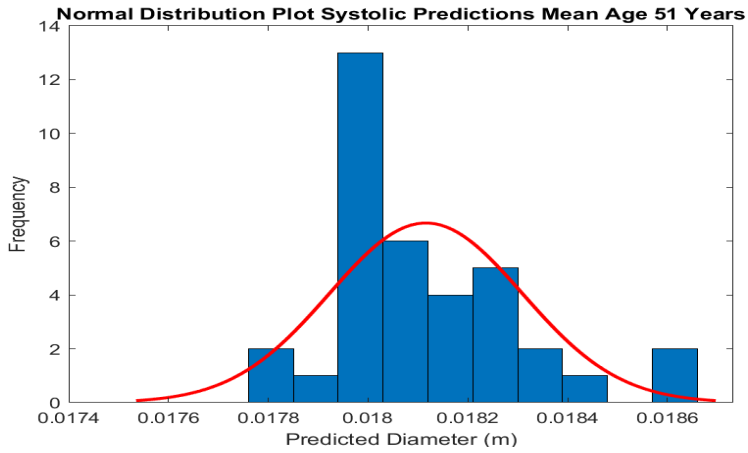

Figure 66: Normal distribution plot of the systolic diameter predictions from the proposed neural network from graph B for mean 51 years

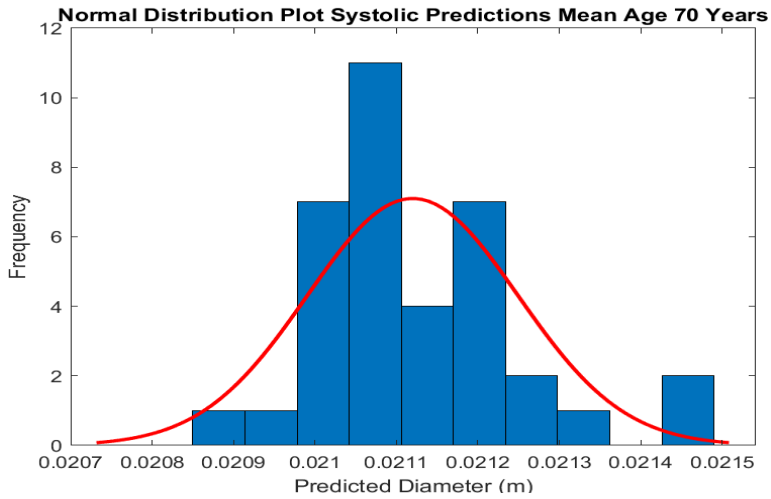

Figure 67: Normal distribution plot of the systolic diameter predictions from the proposed neural network from graph C for mean 70 years

Figure 65, Figure 66, and Figure 67 show that the distributions for the systolic diameter predictions are skewed right. This means that the distribution ranges are not normal, thus the Kruskal-Wallis ANOVA test is the appropriate test to perform on the systolic predicted data.

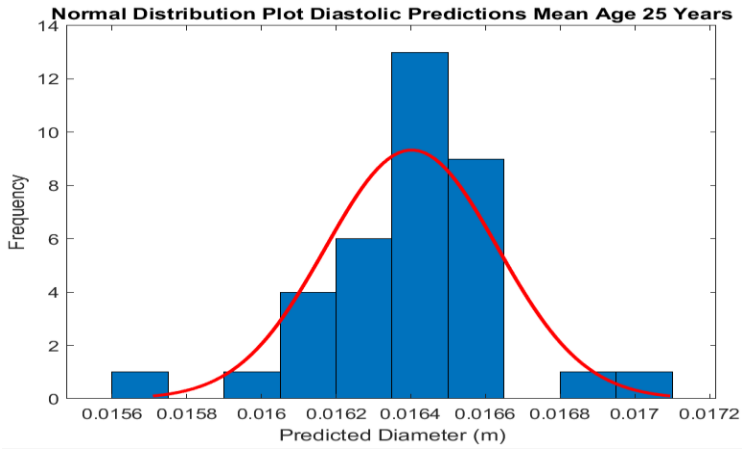

Figure 68: Normal distribution plot of the diastolic diameter predictions from the proposed neural network from graph A for mean 25 years

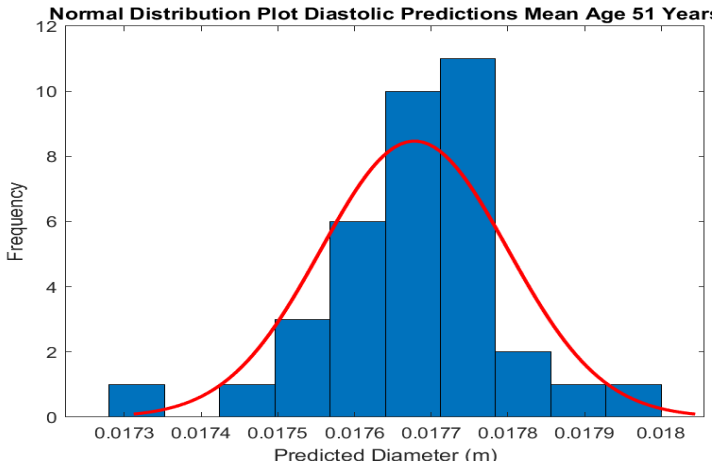

Figure 69: Normal distribution plot of the diastolic diameter predictions from the proposed neural network from graph B for mean 51 years

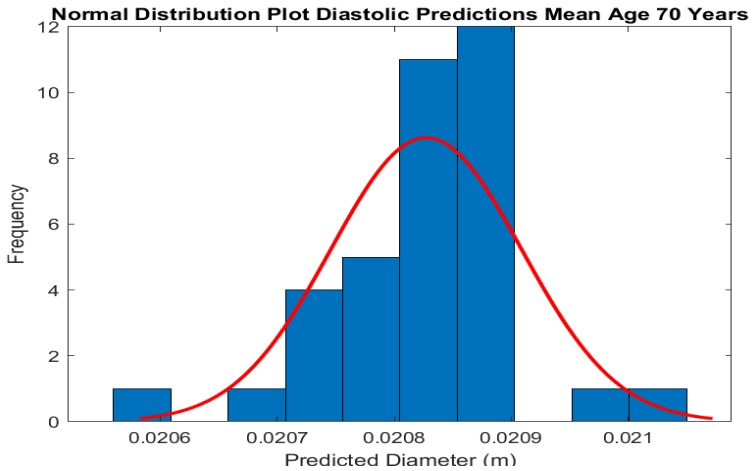

Figure 70: Normal distribution plot of the diastolic diameter predictions from the proposed neural network from graph C for mean 70 years

Figures Figure 68, Figure 69, and Figure 70 show that the distributions for the diastolic diameter predictions are skewed left. This also means that the distribution ranges are not normal, thus the Kruskal-Wallis ANOVA test is the appropriate test to perform on the diastolic predicted data as well.

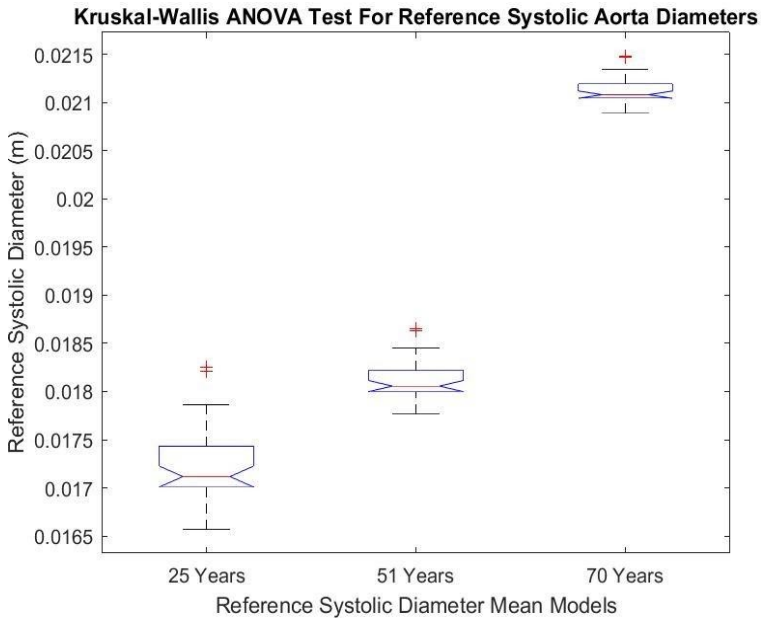

Figure 71: Graph of Kruskal-Wallis ANOVA test for reference systolic aorta diameters

Kruskal-Wallis ANOVA Table

Source	SS	df	MS	Chi-sq	Prob>Chi-sq
Columns	89388.5	2	44694.3	91.12	1.63528e-20
Error	15578.5	105	148.4		
Total	104967	107			

Figure 72: Kruskal-Wallis ANOVA test for reference systolic aorta diameters table data

Figure 71 shows that there are 2 finite outliers observed from the reference systolic diameter models and they were very close in range, so they appear on top of each other. Figure 72 shows that the p value for the systolic models is 1.63528e-20. This means that the null hypothesis is rejected at a 1% significance level, meaning

that there is strong evidence to show that the results come from different populations with the different distribution of aorta diastolic diameters. This makes sense as the aortic diameter sizes largely vary between mean age groups with 25 years having the smallest aortic diameter sizes and 70 years having the largest aortic diameter sizes. Since the p value is much smaller than the significance level tested at these outliers would not impact the conclusions drawn for this data as there would still be a clear difference between the population diameters at different ages.

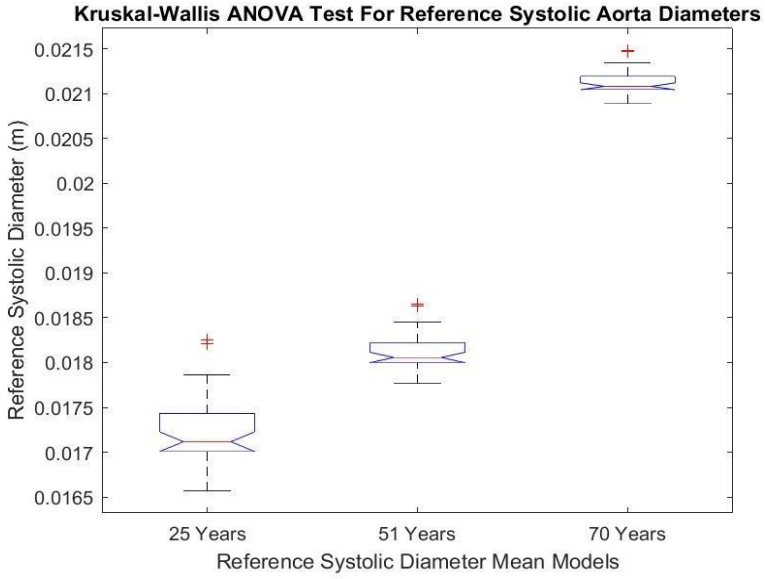

Figure 73: Graph of Kruskal-Wallis ANOVA test for reference diastolic aorta diameters

Kruskal-Wallis ANOVA Table

Source	SS	df	MS	Chi-sq	Prob>Chi-sq
Columns	93312	2	46656	95.12	2.21367e-21
Error	11655	105	111		
Total	104967	107			

Figure 74: Kruskal-Wallis ANOVA test for reference diastolic aorta diameters table data

Figure 73 shows that there are also 2 finite outliers observed from the reference diastolic diameter models, but this time one was a lower outlier, and one was a higher outlier. Figure 74 shows that the p value for the systolic models is 2.21367e-21. This again means that the null hypothesis is rejected at a 1% significance level, meaning that there is strong evidence to show that the results come from different populations with the different distribution of aorta diastolic diameters. This also makes sense as the aortic diameter sizes largely vary between mean age groups with 25 years having the smallest aortic diameter sizes and 70 years having the largest aortic diameter sizes. Since the p value is also much smaller than the significance level tested at these outliers would not impact the conclusions drawn for this data as there would still be a clear difference between the population diameters at different ages.

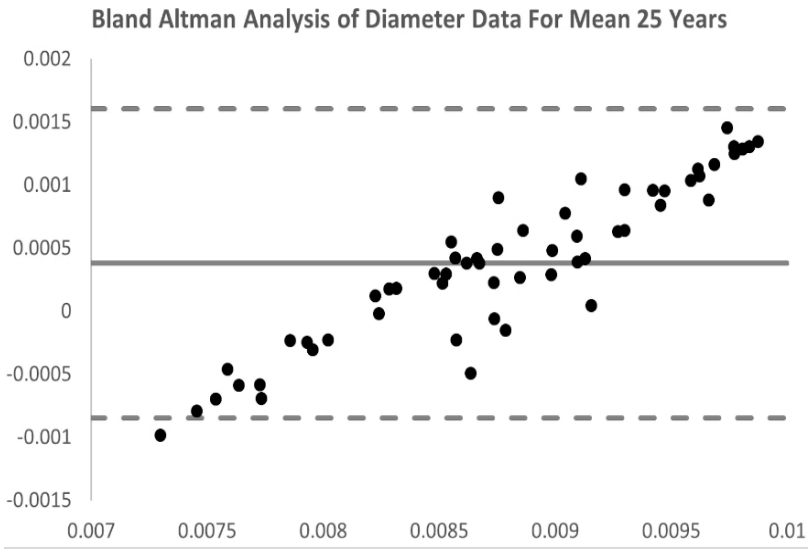

Figure 75: Bland Altman analysis of the predicted diameter data for mean 25 years

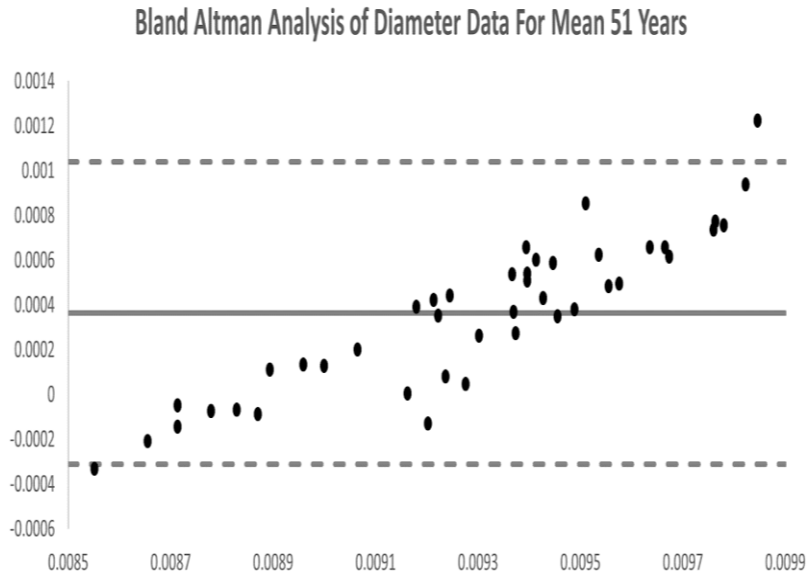

Figure 76: Bland Altman analysis of the predicted diameter data for mean 51 years

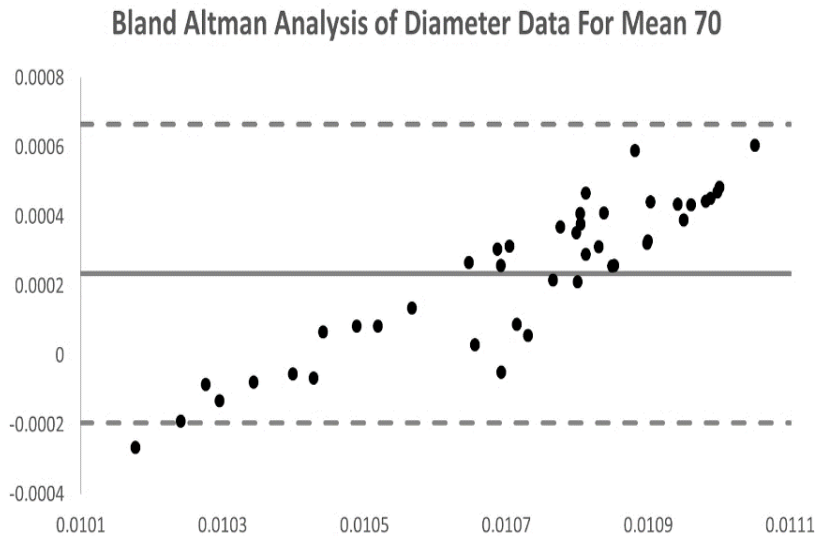

Figure 77: Bland Altman analysis of the predicted diameter data for mean 70 years

Figure 75 and Figure 77 show that only 1 data point falls outside of the 95% limits and Figure 76 shows that only 2 data points falls outside of the 95% limits of agreement. These plots clearly show that over 95% of the data is encompassed in the limits of agreement and have a large linear spread, allowing a conclusion that there is no clear bias seen in the data for the mean age range of 25, 51, or 70 years. These plots also allow one to conclude that there is both a clear relationship as well as no bias between the predicted and reference diameter data collected for all mean age ranges studied by the Länne *et. al* study.

3.5 Uncertainty Analysis

One reason as to why the predicted diameter values do not strongly correlate with the validation data is that the neural network was created using the open sourced HaeMod database to simulate various aortic pressure and flow data. The HaeMod database was utilized as it is very difficult to find a large database that collects all the reference variables that are needed to evaluate cardiovascular system precisely. The HaeMod database, which is free to use, allows for researchers to infer the physiology behind the cardiovascular system through analysis of the pulse wave morphology simulations. This database allows for researchers to openly research new advances in understanding cardiovascular risk without costing them money to perform expensive and invasive clinical trials on human subjects. As this is simulated data, not clinically collected data, this physiological difference could account for the differences in the predicted values versus the reference values observed for aortic systolic and diastolic diameters.

Another reason that the predicted aorta diameter values did not strongly correlate with the reference values may be related to the method of obtaining reference blood pressure waveforms from previously published clinical journals. The waveforms were re-digitized into tabular data of pressure (mmHg) and time (s) using the WebPlotDigitizer app. Errors in digitizing could have arisen from both computer and human error. The computer takes the background color chosen and attempts to

match the waveform using the step with interpolation function there is some room for error as the data points are not always placed directly in the center of the waveform as one would expect. This is where the human error can form as the researcher then has to slowly move through the waveform and either add, delete, or move data points to help obtain the proper waveform desired. As the human eye is not perfectly precise, this could lead to slightly inaccurate waveform readings to be extrapolated, which may contribute to the predictions not correlating strongly with the reference data.

An additional reason for the weaker correlations observed from the neural network could be from only using healthy, normotensive humans to use in the clinical database that was created. As the healthy, normotensive population is not an accurate representation of the entire human race population, this could account for the discrepancies between the predicted and reference diameters. The simulated data in the neural network was trained using a wide range of pressure and flow models while the reference database was constructed using only healthy subjects. This difference may have influenced the resulting moderate correlation observed between the predictions and reference data as only the control population was validated.

One reason that the first validation study could have negatively influenced the correlation study of the predicted versus reference aortic diameters is that this study was published using only one subject. As one subject does not accurately depict

an entire population, in this case healthy individuals with no cardiovascular diseases, the results could be skewed to not correlate with the targeted population we built the database around. This could easily be a contributing factor to the less strongly associated correlation that was observed between both the systolic and diastolic aorta diameter predictions.

On the other hand, the second validation study found did not present raw values but rather the mean pressure and diameter values for men. Clearly, this study does not account for female aorta pressure and diameter relationships, which our database contains, which can help explain some of the correlation uncertainties observed from the neural network. Additionally, only having mean values graphs of overall aorta diameters means that the digitization of the observed curves did not provide exact measurements for systolic and diastolic pressure and flow in the male aorta at different ages, but only the general idea observed for the study. This discrepancy can also explain the lower correlation value observed between the predicted and reference values for both diastolic and systolic aortic diameters as the study did not provide clear data for systolic and diastolic diameters but rather just the mean diameter as a whole.

To utilize the validation data, a linear model was created to predict the systolic and diastolic aortic diameters as it would encompass a large portion of the pressure data observed in human blood pressure observations. The human cardiovascular blood

pressure is not a linear model, thus this computation method could lead to the extremes observed to be ignored in the predictions, thus decreasing the correlation observed between the prediction and the reference diameter values for both the systolic and diastolic aorta. Though the linear model would allow for most of the blood pressure measurements to be utilized in the prediction of systolic and diastolic aortic diameters, there may be unintentional bias from the extreme values that would be exhibited by the true nonlinear relationship that is observed in the human cardiovascular system.

Chapter 4
Conclusions and Future Work

4.1 Conclusion

As the results for the correlation between the predicted systolic and reference systolic values showed moderate correlation, it appears that continuing to build upon the research database could prove to be beneficial for the medical world. Since research has shown that systolic blood pressure is a better indicator for CVD risk than diastolic blood pressure, the results of this validation study gives hope that this neural network model may be good for determining if someone is at a higher risk of developing a CVD in the upcoming years.

With further validation training and testing, that the neural network can be useful in a clinical setting to predict systolic aortic diameter size to evaluate the risk of developing a CVD. This is demonstrated through the study as the systolic diameter correlation gave moderate correlations in regard to the clinical validation data published by the Länne and Stefanadis articles. This finding along with the previous research could help shift further studies into evaluating the systolic pressure and diameters to help determine CVD risk and help doctors prescribe preventative treatments before the person develops a life-threatening CVD. As there is still no widely accepted non-invasive tool to measure aortic diameter in a clinical setting,

there is an urgent need to continue novel methods and research to help physicians slow down the global rate of CVD mortality.

4.2 Future Work

In the future, a larger clinical database that contains age, sex, blood pressure, blood flow, as well as aortic systolic and diastolic diameters should be constructed. This should be done by collaborating with a clinical laboratory or hospital to create a larger database of clinical pressure and flow data to continue to train the neural network. This collaboration would be conducted in hopes of obtaining stronger correlations between both systolic and diastolic aorta diameter values. The database should include subjects that better represent the entire human population of either a certain region or of the global population instead of just the control group. This will allow for the neural network to be trained using real, clinical data as opposed to the simulated pressure and flow data.

References

Afzal, A., Fung, D., Galligan, S., Godwin, E. M., Kral, J. G., Salciccioli, L., & Lazar, J. M. (2014). The effect of lower body weight support on arterial wave reflection in healthy adults. *Journal of the American Society of Hypertension: JASH*, *8*(6), 388–393.

Asia Pacific Cohort Studies. (2003). Blood pressure and cardiovascular disease in the Asia Pacific region. *Journal of Hypertension*, *21*(4), 707–716.

Bae, S., Kim, S. R., Kim, M.-N., Shim, W. J., & Park, S.-M. (2021). Impact of cardiovascular disease and risk factors on fatal outcomes in patients with COVID-19 according to age: A systematic review and meta-analysis. *Heart*, *107*(5), 373–380.

Bansal, M. (2020). Cardiovascular disease and COVID-19. *Diabetes & Metabolic Syndrome: Clinical Research & Reviews*, *14*(3), 247–250.

Benjamin, E. J., Muntner, P., Alonso, A., Bittencourt, M. S., Callaway, C. W., Carson, A. P., Chamberlain, A. M., Chang, A. R., Cheng, S., Das, S. R., Delling, F. N., Djousse, L., Elkind, M. S. V., Ferguson, J. F., Fornage, M., Jordan, L. C., Khan, S. S., Kissela, B. M., Knutson, K. L., … American Heart Association Council on Epidemiology and Prevention Statistics Committee and Stroke Statistics Subcommittee. (2019). Heart Disease and Stroke Statistics-2019 Update: A Report From the American Heart Association. *Circulation*, *139*(10), e56–e528.

Böhm, M., Frey, N., Giannitsis, E., Sliwa, K., & Zeiher, A. M. (2020). Coronavirus Disease 2019 (COVID-19) and its implications for cardiovascular care: Expert document from the German Cardiac Society and the World Heart Federation. *Clinical Research in Cardiology*, *109*(12), 1446–1459.

Chuang Michael L., Gona Philimon N., Qazi Saadia, Musgrave Rebecca M., Fox Caroline S., Massaro Joseph M., Hoffmann Udo, & O'Donnell Christopher J. (2018). Aortic Arch Width and Cardiovascular Disease in Men and Women in the Community. *Journal of the American Heart Association*, *7*(12), e008057.

Clerkin, K. J., Fried, J. A., Raikhelkar, J., Sayer, G., Griffin, J. M., Masoumi, A., Jain, S. S., Burkhoff, D., Kumaraiah, D., Rabbani, L., Schwartz, A., & Uriel, N. (2020). COVID-19 and Cardiovascular Disease. *Circulation*, *141*(20), 1648–1655.

Damen, J. A. A. G., Hooft, L., Schuit, E., Debray, T. P. A., Collins, G. S., Tzoulaki, I., Lassale, C. M., Siontis, G. C. M., Chiocchia, V., Roberts, C., Schlüssel, M. M., Gerry, S., Black, J. A., Heus, P., Schouw, Y. T. van der, Peelen, L. M., & Moons, K. G. M. (2016). Prediction models for cardiovascular disease risk in the general population: Systematic review. *BMJ*, *353*, i2416.

Dongare, A. D., Kharde, R. R., & Kachare, A. D. (2012). Introduction to Artificial Neural Network. *International Journal of Engineering and Innovative Technology*, *2*(1), 6.

Elvan-Taşpinar, A., Franx, A., Bots, M., Bruinse, H., & Koomans, H. (2004). Central Hemodynamics of hypertensive disorders in pregnancy. *American Journal of Hypertension*, *17*, 941–946.

Garcia Mariana, Mulvagh Sharon L., Bairey Merz C. Noel, Buring Julie E., & Manson JoAnn E. (2016). Cardiovascular Disease in Women. *Circulation Research*, *118*(8), 1273–1293.

Gaziano, J. M., & Manson, J. E. (1996). DIET AND HEART DISEASE: The Role of Fat, Alcohol, and Antioxidants. *Cardiology Clinics*, *14*(1), 69–83.

Giavarina, D. (2015). Understanding Bland Altman analysis. *Biochemia Medica*, *25*(2), 141–151.

Glasser, S. P., Arnett, D. K., McVeigh, G. E., Finkelstein, S. M., Bank, A. J., Morgan, D. J., & Cohn, J. N. (1997). Vascular Compliance and Cardiovascular Disease: A Risk Factor or a Marker? *American Journal of Hypertension*, *10*(10), 1175–1189.

Hecke, T. V. (2012). Power study of anova versus Kruskal-Wallis test. *Journal of Statistics and Management Systems*, *15*(2–3), 241–247.

Holt Zaugg, R. E. W., Isaku Tateishi, Daniel L. Randall. (2011). Mendeley: Creating Communities of Scholarly Inquiry Through Research Collaboration. *TechTrends*, *55*(1), 32–36.

Hrušková, J. (2015, September 9). *Calculation of the Pulse Wave Velocity from the Waveform of the Central Aortic Pressure Pulse in Young Adults*.

Kaya, M., Balasubramanian, V., Patel, A., Ge, Y., & Li, J. K.-J. (2018). A novel compliance-pressure loop approach to quantify arterial compliance in systole and in diastole. *Computers in Biology and Medicine*, *99*, 98–106.

Kengne Andre-Pascal, Czernichow Sébastien, Huxley Rachel, Grobbee Diederick, Woodward Mark, Neal Bruce, Zoungas Sophia, Cooper Mark, Glasziou Paul, Hamet Pavel, Harrap Stephen B., Mancia Giuseppe, Poulter Neil, Williams Bryan, & Chalmers John. (2009). Blood Pressure Variables and Cardiovascular Risk. *Hypertension*, *54*(2), 399–404.

Länne, T., Sonesson, B., Bergqvist, D., Bengtsson, H., & Gustafsson, D. (1992). Diameter and compliance in the male human abdominal aorta: Influence of age and aortic aneurysm. *European Journal of Vascular Surgery*, *6*(2), 178–184.

Laughlin, G. A., Allison, M. A., Jensky, N., Aboyans, V., Wong, N. D., Detrano, R., & Criqui, M. H. (2011). Abdominal Aortic Diameter and Vascular Atherosclerosis: The Multi-Ethnic Study of Atherosclerosis. *European Journal of Vascular and Endovascular Surgery : The Official Journal of the European Society for Vascular Surgery*, *41*(4), 481–487.

Lee, B.-K. (2011). Computational Fluid Dynamics in Cardiovascular Disease. *Korean Circulation Journal*, *41*(8), 423.

Li, J. K.-J., & Zhu, Y. (1994). Arterial Compliance and Its Pressure Dependence in Hypertension and Vasodilation. *Angiology*, *45*(2), 113–117.

Lim, M. A., & Townsend, R. R. (2009). Arterial compliance in the elderly: Its effect on blood pressure measurement and cardiovascular outcomes. *Clinics in Geriatric Medicine*, *25*(2), 191–205.

Lloyd-Jones Donald M., Hong Yuling, Labarthe Darwin, Mozaffarian Dariush, Appel Lawrence J., Van Horn Linda, Greenlund Kurt, Daniels Stephen, Nichol Graham, Tomaselli Gordon F., Arnett Donna K., Fonarow Gregg C., Ho P. Michael, Lauer Michael S., Masoudi Frederick A., Robertson Rose Marie, Roger Véronique, Schwamm Lee H., Sorlie Paul, … Rosamond Wayne D. (2010). Defining and Setting National Goals for Cardiovascular Health Promotion and Disease Reduction. *Circulation*, *121*(4), 586–613.

Lowe, A., Harrison, W., El-Aklouk, E., Ruygrok, P., & Al-Jumaily, A. M. (2009). Non-invasive model-based estimation of aortic pulse pressure using suprasystolic brachial pressure waveforms. *Journal of Biomechanics*, *42*(13), 2111–2115.

Mao, S. S., Ahmadi, N., Shah, B., Beckmann, D., Chen, A., Ngo, L., Flores, F. R., Gao, Y. lin, & Budoff, M. J. (2008). Normal Thoracic Aorta Diameter on Cardiac Computed Tomography in Healthy Asymptomatic Adult; Impact of Age and Gender. *Academic Radiology*, *15*(7), 827–834.

Marin, F., Rohatgi, A., & Charlot, S. (2017). WebPlotDigitizer, a polyvalent and free software to extract spectra from old astronomical publications: Application to ultraviolet spectropolarimetry. *French Society of Astronomy & Astrophysics,* ArXiv:1708.02025, 237-241.

Matthys, K. S., Alastruey, J., Peiró, J., Khir, A. W., Segers, P., Verdonck, P. R., Parker, K. H., & Sherwin, S. J. (2007). Pulse wave propagation in a model human arterial network: Assessment of 1-D numerical simulations against in vitro measurements. *Journal of Biomechanics*, *40*(15), 3476–3486.

Mehta, N. K., Abrams, L. R., & Myrskylä, M. (2020). US life expectancy stalls due to cardiovascular disease, not drug deaths. *Proceedings of the National Academy of Sciences*, *117*(13), 6998–7000.

Murgo, J. P., Westerhof, N., Giolma, J. P., & Altobelli, S. A. (1981). Manipulation of ascending aortic pressure and flow wave reflections with the Valsalva maneuver: Relationship to input impedance. *Circulation*, *63*(1), 122–132.

Narayan, O., Li, Q., Curry, G., Coombs, P., Mottram, P., Meredith, I., & Cameron, J. (2013). Timing of the Aortic Pulse Wave Inflection Point is Associated with Mitral Annular Systolic Motion. *Heart, Lung and Circulation*, *22*, S28–S29.

Nichols, W., Petersen, J., Denardo, S., & Christou, D. (2013). Arterial stiffness, wave reflection amplitude and left ventricular afterload are increased in overweight individuals. *Artery Research*, *7*, 222–229.

Nichols, W. W. (2005). Clinical measurement of arterial stiffness obtained from non-invasive pressure waveforms. *American Journal of Hypertension*, *18*(1 Pt 2), 3S-10S.

Oparil, S., Acelajado, M. C., Bakris, G. L., Berlowitz, D. R., Cífková, R., Dominiczak, A. F., Grassi, G., Jordan, J., Poulter, N. R., Rodgers, A., & Whelton, P. K. (2018). Hypertension. *Nature Reviews. Disease Primers*, *4*, 18014.

O'Rourke, M. F., & Adji, A. (2008). Basis for use of central blood pressure measurement in office clinical practice. *Journal of the American Society of Hypertension: JASH*, *2*(1), 28–38.

O'Rourke, M. F., & Hashimoto, J. (2007). Mechanical factors in arterial aging: A clinical perspective. *Journal of the American College of Cardiology*, *50*(1), 1–13.

O'Rourke, M. F., & Seward, J. B. (2006). Central arterial pressure and arterial pressure pulse: New views entering the second century after Korotkov. *Mayo Clinic Proceedings*, *81*(8), 1057–1068.

Paul, T. K., Alamin, A. E., Subedi, P., Alamian, A., Wang, L., Blackwell, G., Budoff, M., & Mamudu, H. M. (2020). Association Between Cardiovascular Risk Factors and the Diameter of the Thoracic Aorta in an Asymptomatic Population in the Central Appalachian Region. *The American Journal of the Medical Sciences*, *361*(2), 202–207.

Qazi Saadia, Massaro Joseph M., Chuang Michael L., D'Agostino Ralph B., Hoffmann Udo, & O'Donnell Christopher J. (2017). Increased Aortic Diameters on Multidetector Computed Tomographic Scan Are Independent Predictors of Incident Adverse Cardiovascular Events. *Circulation: Cardiovascular Imaging*, *10*(12), e006776.

Schmidhuber, J. (2015). Deep learning in neural networks: An overview. *Neural Networks*, *61*, 85–117.

Smith, S. A., Morris, J. M., & Gallery, E. D. m. (2004). Methods of assessment of the arterial pulse wave in normal human pregnancy. *American Journal of Obstetrics and Gynecology*, *190*(2), 472–476.

Staessen, J. A., Li, Y., Hara, A., Asayama, K., Dolan, E., & O'Brien, E. (2017). Blood Pressure Measurement Anno 2016. *American Journal of Hypertension*, *30*(5), 453–463.

Stefanadis Christodoulos, Stratos Costas, Vlachopoulos Charalambos, Marakas Stelios, Boudoulas Harisios, Kallikazaros Ioannis, Tsiamis Eleftherios, Toutouzas Konstantinos, Sioros Lambros, & Toutouzas Pavlos. (1995). Pressure-Diameter Relation of the Human Aorta. *Circulation*, *92*(8), 2210–2219.

Subherwal, S., de las Fuentes, L., Waggoner, A. D., Heuerman, S., Spence, K. E., & Davila-Roman, V. G. (2010). Central Aortic Pressure is Independently Associated With Diastolic Function. *American Heart Journal*, *159*(6), 1081–1088.

The Center for Disease Control and Prevention. (2019, August 16). *Heart Disease Death Rates Aged 35 and older, Total Population*. Centers for Disease Control and Prevention. https://www.cdc.gov/dhdsp/maps/national_maps/hd_all.htm

The Center for Disease Control and Prevention. (2020, September 8). *Heart Disease Facts*. Centers for Disease Control and Prevention. https://www.cdc.gov/heartdisease/facts.htm

Townsend, R. R., Black, H. R., Chirinos, J. A., Feig, P. U., Ferdinand, K. C., Germain, M., Rosendorff, C., Steigerwalt, S. P., & Stepanek, J. A. (2015). Clinical Use of Pulse Wave Analysis: Proceedings From a Symposium Sponsored by North American Artery. *Journal of Clinical Hypertension (Greenwich, Conn.)*, *17*(7), 503–513.

Townsend, R. R., Rosendorff, C., Nichols, W. W., Edwards, D. G., Chirinos, J. A., Fernhall, B., & Cushman, W. C. (2016). American Society of Hypertension position paper: Central blood pressure waveforms in health and disease. *Journal of the American Society of Hypertension: JASH*, *10*(1), 22–33.

Van Varik, B., Rennenberg, R., Reutelingsperger, C., Kroon, A., De Leeuw, P., & Schurgers, L. (2012). Mechanisms of arterial remodeling: Lessons from genetic diseases. *Frontiers in Genetics*, *3*, 290.

Westerhof B. E., Guelen I., Westerhof N., Karemaker J. M., & Avolio A.. (2006). Quantification of Wave Reflection in the Human Aorta From Pressure Alone. *Hypertension*, *48*(4), 595–601.

Westerhof, N., Lankhaar, J.-W., & Westerhof, B. E. (2009). The arterial Windkessel. *Medical & Biological Engineering & Computing*, *47*(2), 131–141.

Willemet, M., Chowienczyk, P., & Alastruey, J. (2015). A database of virtual healthy subjects to assess the accuracy of foot-to-foot pulse wave velocities for estimation of aortic stiffness. *American Journal of Physiology-Heart and Circulatory Physiology*, *309*(4), H663–H675.

Williams, B., Lacy, P. S., Yan, P., Hwee, C.-N., Liang, C., & Ting, C.-M. (2011). Development and validation of a novel method to derive central aortic systolic pressure from the radial pressure waveform using an n-point moving average method. *Journal of the American College of Cardiology*, *57*(8), 951–961.

World Health Organization. (2020, December 9). *The top 10 causes of death*. https://www.who.int/news-room/fact-sheets/detail/the-top-10-causes-of-death

Wilkins, E., Wilson, L., Wickramasinghe, K., Bhatnagar, P., Leal, J., Luengo-Fernandez, R., Burns, R., Rayner, M., & Townsend, N. (2017). European Cardiovascular Disease Statistics 2017. *European Heart Network, Brussels*, 1-192.